Neurobiology of Disease 224 (2026) 107396

Contents lists available at ScienceDirect

Neurobiology of Disease

journal homepage: www.elsevier.com/locate/ynbdi

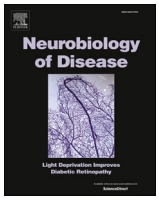

Elucidation of the influence of the $Ca_V2.2$ calcium channel on ALS disease progression in the SOD1*G93A mouse model

Katharina Wintz [a,b], Paul Luca Lechtape [a], Jannes Klenzendorf [a], Sarah Schemmert [b], Andrew J. Dingley [a,b], Antje Willuweit [c], Janine Kutzsche [b,*]

[a] Institut für Physikalische Biologie, Heinrich Heine University Düsseldorf, Faculty of Mathematics and Natural Sciences, Universitätsstraße 1, 40225 Düsseldorf, Germany
[b] Institute of Biological Information Processing, Structural Biochemistry (IBI-7), Forschungszentrum Jülich GmbH, Wilhelm-Johnen-Straße, 52428 Jülich, Germany
[c] Institute of Neuroscience and Medicine, Medical Imaging Physics (INM-4), Forschungszentrum Jülich GmbH, Wilhelm-Johnen-Straße, 52428 Jülich, Germany

ARTICLE INFO

Keywords:
Amyotrophic lateral sclerosis
Behavior
Motor coordination
$Ca_V2.2$
SOD1*G93A
Double-transgenic mice

ABSTRACT

Amyotrophic lateral sclerosis (ALS) is a late-onset, fatal neurodegenerative disease affecting upper and lower motor neurons in the central nervous system. Drugs like riluzole, edaravone, and tofersen treat disease symptoms or are designed for a specific pathological mutation (e.g., SOD1), but they cannot prevent or halt the disease. For this reason, the search for new therapeutic strategies continues. The voltage-gated calcium channel $Ca_V2.2$ might be a novel target in ALS treatment as the channel was shown to be overexpressed in murine SOD1*G93A cortical neurons, resulting in higher mortality. Further, murine SOD1*G93A motor neurons showed increased calcium currents mainly by an increased expression of the $Ca_V2.2$ channel. In addition, inhibition of the channel was hypothesized as mode of action for the all-D-enantiomeric peptide RD2RD2, a novel drug candidate for the treatment of ALS, which already demonstrated its efficacy in SOD1*G93A mice. To investigate the influence of the $Ca_V2.2$ channel on the progression of disease symptoms in the SOD1*G93A mouse model, a new double-transgenic line was created, combining the ALS phenotype with a knockout of the $Ca_V2.2$ channel.

The study showed that the $Ca_V2.2$ knockout on the SOD1*G93A background led to reduced SHIRPA and splay scores, and a delayed disease onset. Additionally, differences were detected between wildtype and single-transgenic $Ca_V2.2$ knockout mice. However, survival was not affected. Post mortem analysis of human tissue found more $Ca_V2.2$ in ALS cases in comparison to healthy control subjects confirming involvement of the channel in human ALS. These results indicate that the $Ca_V2.2$ calcium channel may play an influential role in early disease progression of ALS.

1. Introduction

Amyotrophic lateral sclerosis (ALS) is a late-onset neurodegenerative disease that affects both upper and lower motor neurons. Early symptoms include muscle weakness, spasms, atrophy, and cramps that gradually spread to neighboring muscles during disease progression (Masrori and Van Damme, 2020). The site of onset is typically classified as limb onset (65%), bulbar onset (30%) or respiratory onset (5%) (Hardiman et al., 2011). Disease progression ultimately leads to the loss of whole muscle function and the inability of patients to communicate with their environment, resulting in the so-called totally-locked-in state. Most patients die from respiratory arrest 3–5 years after diagnosis (Zarei et al., 2015). In the majority of cases the cause is unknown (i.e., sporadic ALS, sALS), whereas ~10% of cases are associated with inherited genetic mutations (i.e., familial ALS, fALS) (Masrori and Van Damme, 2020). Currently, 18 genes are considered to be definitively associated with ALS (ALSoD A, 2022). Among these, fused in sarcoma (*FUS*), TAR DNA-binding protein 43 (*TARDBP*), chromosome 9 open reading frame 72 (*C9orf72*), and Cu/Zn-superoxide dismutase1 (*SOD1*) belong to the most frequently mutated genes in fALS (Masrori and Van Damme, 2020). The identification of these genes enabled the development of ALS-specific mouse models. In 1994, Gurney et al. (Gurney et al., 1994) established the first ALS mouse line, B6.Cg-Tg(SOD1*G93A)1Gur/J, based on the SOD1*G93A mutation. SOD1*G93A mice exhibit hallmark features

* Corresponding author at: Institute of Biological Information Processing, Structural Biochemistry (IBI-7), 52425 Jülich, Germany.
E-mail addresses: k.wintz@fz-juelich.de (K. Wintz), jannes.klenzendorf@hhu.de (J. Klenzendorf), sarah.schemmert@priavoid.com (S. Schemmert), a.dingley@fz-juelich.de (A.J. Dingley), a.willuweit@fz-juelich.de (A. Willuweit), j.kutzsche@fz-juelich.de (J. Kutzsche).

https://doi.org/10.1016/j.nbd.2026.107396
Received 8 January 2026; Received in revised form 19 March 2026; Accepted 10 April 2026
Available online 13 April 2026

of ALS, including loss of choline acetyltransferase (ChAT)-positive motor neurons, neurofilament accumulation, gliosis, and progressive hind limb weakness that reaches total hind limb paralysis thereby mimicking key aspects of human ALS pathology (Gurney et al., 1994; Mead et al., 2011).

Currently, four drugs are approved by the U.S. Food and Drug Administration (FDA) for treating ALS (ALS Association T, 2026). These therapies do not halt disease progression, but slow functional decline and/or extend survival up to three months. Prominent examples include riluzole, which reduces glutamate excitotoxicity, and edaravone, a free radical scavenger (Jaiswal, 2019). These drugs target underlying disease mechanisms in ALS. One mechanism involves glutamate excitotoxicity, in which excessive neurotransmitter release triggers neuronal cell death signaling (Suzuki et al., 2022). Another mechanism is oxidative stress caused by the abnormal production of reactive oxygen species (ROS), leading to the formation of radicals and subsequent cellular damage (Park and Yang, 2021). The drug AMX0035, a combination of phenylbutyrate and taurursodiol designed to simultaneously target mitochondrial dysfunction and endoplasmic reticulum (ER) stress (Paganoni et al., 2020; Paganoni et al., 2021), was initially approved by the FDA but later withdrawn by the manufacturer following a negative phase III clinical trial (Ketabforoush et al., 2024). Additional disease mechanisms implicated in ALS include neuroinflammation mediated by glial cells (You et al., 2023) and protein aggregation (Gosset et al., 2022). For specific cases of SOD1-associated ALS, the antisense oligonucleotide drug tofersen was recently approved by the FDA (Miller et al., 2022).

The voltage-gated calcium channel $Ca_V2.2$ (N-type) is located in dendritic and presynaptic membranes, where it regulates the Ca^{2+} influx required for neurotransmitter release (Jurkovicova-Tarabova and Lacinova, 2019). These channels are also expressed in glial cells, where they contribute to calcium homeostasis and thereby influence inflammatory responses (Huntula et al., 2019). A $Ca_V2.2$ knockout (KO) mouse model was established by Saegusa et al., 2001. These mice displayed reduced anxiety-linked behavior and diminished responses to inflammatory and neuropathic pain in behavioral assays, while otherwise appearing largely similar to wild-type (WT) animals (Saegusa et al., 2001).

Calcium dysregulation, neuroinflammation, and glutamate excitotoxicity are important disease mechanisms in ALS that may be affected or regulated by the N-type calcium channel thereby linking $Ca_V2.2$ to ALS. Pieri and colleagues provided the first evidence that $Ca_V2.2$ may be involved in early progression of ALS (Pieri et al., 2013). They reported increased calcium channel expression in cultured cortical neurons from SOD1*G93A mice, which was associated with higher neuronal mortality. The authors proposed that elevated $Ca_V2.2$ density may enhance neurotransmitter release, resulting in hyperexcitability. Chang et al. subsequently isolated spinal motor neurons from SOD1*G93A mouse embryos and observed increased $Ca_V2.2$ expression at the plasma membrane of soma and dendrites together with high-voltage-activated Ca^{2+} currents (Chang and Martin, 2016). In addition, treatment with the potential drug candidate RD2RD2, an all-D-enantiomeric peptide, reduced motor symptoms and delayed disease onset in SOD1*G93A mice (Post et al., 2021a; Post et al., 2021b). These effects may involve inhibiting the $Ca_V2.2$ channel, as the lead compound RD2 was shown to inhibit this channel (IC_{50}: 0.15 μM, K_D: 0.12 μM) (Kutzsche et al., 2024). By combining the findings of Pieri and Chang and our own observations, these studies suggest that $Ca_V2.2$ may influence early ALS pathology in the SOD1*G93A mouse model.

In this report, we present a characterization study of a newly generated double-transgenic mouse line that combines the ALS model SOD1*G93A with a KO of the N-type calcium channel. This model was developed to test the hypothesis that $Ca_V2.2$ contributes to ALS disease progression.

2. Methods

2.1. Animals

Male mice of the congenic B6.Cg-Tg(SOD1*G93A)1Gur/J line (short SOD1) were purchased from JAX (strain: 004435, The Jackson Laboratory, Bar Harbor, ME, USA) and bred in-house with C57BL/6J females obtained from CRIVER (strain: 632, Charles River Laboratories, Sulzfeld, Germany). Heterozygous mice of the B6;129S4-Cacna1b^{tm1Ttan} line (short $Ca_v2.2^{+/-}$) were obtained from RIKEN (strain: RBRC04884, Riken BRC Experimental Animal Division, Tsukuba, Ibaraki, Japan) and bred in-house with the same C57BL/6J mice. In the first step, heterozygous SOD1 mice were bred with heterozygous $Cav2.2^{+/-}$ mice to obtain double-heterozygous $Ca_V2.2^{+/-}$-SOD1 mice. In the second step, these mice were bred again with heterozygous $Ca_V2.2^{+/-}$ mice to obtain double-transgenic $Ca_v2.2^{-/-}$-SOD1 mice (here $Cav^{-/-}$-SOD1 mice). Each mouse was genotyped with DNA extracted from ear tissue collected at P21. The SOD1 genotype and copy number were analyzed by RT-PCR as previously described (Alexander et al., 2004) prior to starting the study to ensure stable phenotype progression. The $Ca_v2.2$ genotype was determined by PCR.

At the Forschungszentrum Jülich animal facility, mice were housed under a controlled specific-pathogen-free (SPF) environment (12/12 h light/dark cycle, humidity maintained around 50%, room temperature between 20 °C and 23 °C). Prior to entering the SPF area, food, water, and cages were autoclaved. A maximum of five mice were housed in individually ventilated cages on standardized rodent bedding (Rettenmaier, Rosenberg, Germany). Tap water and dried, pelleted standard rodent chow (Altromin, Lage, Germany) were available for the animals ad libitum. After disease onset, nutrition of the animals was ensured by dissolving powdered food pellets in drinking water in a small container on the cage floor.

2.2. Study design

A power analysis was conducted based on differences in the splay test between SOD1 and WT mice reported in a previous study (Post et al., 2021b). For $n = 14$, a statistical power of 84% was calculated. Because of the non-mendelian distribution of the $Cav^{-/-}$-SOD1 genotype during breeding, the study was divided into two parts. In total, 13 transgenic SOD1 mice (7♂:6♀), 14 homozygous $Cav^{-/-}$ mice (7♂:7♀), 13 double-transgenic $Cav^{-/-}$-SOD1 mice (8♂:6♀), and 13 non-transgenic WT mice (7♂:7♀) were included. The gender distribution was balanced within each group and between groups, if not restricted by the total number of available mice of the genotype ($Cav^{-/-}$-SOD1). One female SOD1 mouse was excluded from the analysis. In the first part of the study, weekly motor tests were conducted from 6 to 21 weeks of age. These tests included the SmithKline Beecham, Harwell, Imperial College, Royal London Hospital, phenotype assessment (SHIRPA) test, the splay reflex test, the modified pole test, and the four-limb hanging wire test. Additionally, the open field test (OFT) was performed every fourth week.

The second part of the study followed the same experimental design but included additional tests to better describe the non-WT-like behavior of the $Cav^{-/-}$ mice. Additional behavioral tests every fourth week included the object exploration test and the rotarod test. Moreover, grip strength measurements were performed every fourth week and weekly after disease onset. To assess behavior in the experimental cage during the testing days, the gnawing behavior on paper tissues was analyzed using image analysis.

Body weight and general health were monitored three times per week. After disease onset, affected mice were monitored daily to assess termination criteria. Mice reaching predefined end-point criteria were euthanized, and the survival rate was determined for the SOD1 and the $Cav^{-/-}$-SOD1 mice. The experimenter was blinded to genotypes during behavioral testing until ALS-like symptoms became apparent in SOD1

and Cav$^{-/-}$-SOD1 animals, which enabled differentiation between ALS and non-ALS animals.

2.3. Behavioral and motoric tests

2.3.1. SHIRPA phenotype assessment

The SHIRPA assessment is a test battery consisting of several motoric and behavioral test (for details see (Post et al., 2021a)). Each test was scored on a scale from 0 to 3 (0 = WT-like; 3 = extremely different from WT). Individual scores were summed to generate a SHIRPA score sum for comparison among genotypes. Additionally, motor specific tests were summed to form a SHIRPA motor score sum. The SHIRPA test was conducted weekly from week 6 to week 21.

2.3.2. Splay reflex test of hind limbs

The splay reflex test assesses the ability of mice to stretch their hind limbs. In ALS pathology, progressive motoric deficits lead to the gradual loss of this reflex. It was evaluated by a scoring system (0 = WT-like, 1 = reduced splay reflex; 2 = minimal splay reflex, 3 = total loss of splay reflex). The test was repeated three times and the scores were summed for analysis. This test was conducted weekly from week 6 to week 21.

2.3.3. Modified pole test

The modified pole test (Dunkelmann et al., 2018) evaluates the motor coordination and grip strength. Mice were placed head-downwards on a rough-surface pole. A scoring system from 0 to 3 (0 = WT-like, 1 = altered locomotion, 2 = sliding down the pole, 3 = falling down the pole) was used. Each mouse performed three trials and the scores were summed for analysis. The test was conducted weekly between 6 and 21 weeks of age.

2.3.4. Four-limb hanging wire test

In the four-limb hanging wire test, the mice were placed upside down on a grid at a height of approximately 50 cm. The test evaluated the grip and muscle strength of the animals. To prevent injuries when the mice fall, a cage with 10 cm rodent bedding was placed on the bottom of the experimental set up. In the first part of the study, this test was conducted once for a period of 300 s. In the second part of the study, the test was changed to a 3-time repetition of 100 s each to improve meaningfulness of the results. The latency to fall was recorded to compare the different genotypes. The test belonged to the weekly tests from week 6 to week 21.

2.3.5. Open field test

For the OFT, mice were placed in a cubic arena (45 cm × 45 cm) and recorded for 30 min. The arena was divided into a center and a border zone to evaluate anxiety-related and exploratory behavior. Videos were analyzed using EthoVision 15.0 (Wageningen, The Netherlands) to determine parameters such as exploration time, time spent moving, and total distance moved. The OFT was conducted every fourth week (weeks 6, 10, 14, and 18 of age).

2.3.6. Object exploration test

The object exploration test used the same experimental set-up and analysis as the OFT, and was therefore conducted immediately afterward. Mice were briefly removed from the arena, while a cuboid object (6 cm × 6 cm × 15 cm) was placed in the center. Mice were then returned to the arena and exploratory behavior was recorded for 10 min. The test was repeated every fourth week (see OFT schedule) and only during part 2 of the study.

2.3.7. Rotarod

The rotarod is a test for forced motor coordination of mice (Rotarod 47600, Ugo Basile, Gemonio, Italy). The mice were placed on an accelerating rod (4 rpm to 40 rpm) for 5 min. Latency to fall was recorded across three trials and the mean latency was used for analysis. This test was conducted every fourth week (week 7, 11, 15, and 19 of age) and only during part 2 of the study.

2.3.8. Grip strength

Grip strength was measured using a grip strength meter (47200 Ugo Basile, Gemonio, Italy). Mice grasped a plastic grid while being gently pulled backwards until release. The device recorded peak grip force. Each mouse performed three trials, and mean peak force values were used for comparison between genotypes.

2.3.9. Gnawing analysis

During weekly experiments, mice were housed individually and provided with a paper tissue for occupation, nesting, and warmth. At the end of the day, the tissues were removed, flattened on a dark background, and photographed under standardized conditions including a scale bar. The images were processed digitally. Initially, the images were converted into black and white, and then processed using ImageJ (version 1.50b, (Schneider et al., 2012)). A scale was defined using the scale bar and a threshold was applied. The remaining tissue area was then quantified using area measurements to assess gnawing behavior.

2.4. Disease onset and survival analysis

Disease onset in the ALS mouse model was defined according to Mead et al. (Mead et al., 2011) as “the point at which defects in hind limb splay and enhanced tremor were observed with a score of at least 1 in each category”. SOD1 and Cav$^{-/-}$-SOD1 mice meeting these criteria were assigned a phenotype-specific score change from 0 to 1. This time point was marked as the age of disease onset. Survival analysis was performed by comparing the age at euthanasia due to reaching end point criteria between SOD1 and Cav$^{-/-}$-SOD1 mice. End point criteria included body weight loss exceeding 18%, partial paralysis of one or more hind limbs lasting more than 36 h, and/or loss of righting reflex.

2.5. Tissue collection

When mice reached the end point criteria they were euthanized. The brain, the spinal cord, and the *Musculus gastrocnemius* were dissected and placed in 4% PFA solution for 1–3 days. The tissue was then incubated in 30% sucrose for 24 h and stored at –80°C until further use.

2.6. Immunohistochemistry and quantification

For immunohistochemistry, the spinal cord, brain, and muscle tissues of six animals per group were sectioned with a cryostat (CM3050 S Cryostat, Leica, Wetzlar, Germany). Sections of 20 µm thickness were mounted on microscope slides and stored at –80°C until immunohistochemistry. For all tissues, four slides per animal were stained (for muscle tissue two slides per animal were stained, with two images taken per slide). Spinal cord images were taken in the lumbar regions focusing on the ventral horn. Brain regions were selected to include the trigeminal motor nucleus and the facial motor nucleus.

For the immunohistochemistry of the tissues, the following markers were used: (a) neuronal nuclei (NeuN) and glial fibrillary acidic protein (GFAP); (b) SOD1; (c) ChAT and Ionized calcium-binding adaptor molecule 1 (Iba1); (d) ChAT and α-bungarotoxin (Bgtx). For staining procedure (a), an antigen retrieval was performed with 70% formic acid for 5 min. Then, the tissue was incubated with the primary antibodies, rabbit-anti-GFAP 1:1000 (Z0334, Agilent Dako, Santa Clara, CA, USA) and mouse-anti-NeuN 1:1000 (MAB377, KGaA, Darmstadt, Germany), overnight at 4 °C. The following day, the secondary antibody was incubated for 2 h at room temperature and nuclei were counterstained with DAPI.

For the staining procedures (b) and (c), antigen retrieval consisted of 30 min incubation with 10 mM citrate buffer (pH 6) at 80 °C. For staining procedure (d), no antigen retrieval was performed.

Additionally, a 2-h blocking step was included with neutral goat serum for (b) and donkey serum for (c) and (d). SOD1 aggregates were stained with 1:500 rabbit-anti-SOD1 (10269-1-AP, Proteintech Group, Inc., Rosemont, IL, USA). Motor neurons were stained with 1:200 goat-anti-ChAT (NBP1-30052, Novus Biologicals USA, Centennial, CO, USA) and microglia with 1:500 rabbit-anti-Iba1 (019–19,741, FUJIFILM Wako Pure Chemical Corporation, Osaka, Japan). The 488 fluorophore-conjugated Bgtx (B13422, Invitrogen by Thermo Fisher Scientific Inc., Waltham, MA, USA) was incubated with the secondary antibody for (d).

Quantification of neuronal counts in the lumbar spinal cord and brain was performed using ImageJ (version 1.50b, (Schneider et al., 2012)). Cell counts were determined with the *Analyze Particles* function. GFAP, Iba1, and SOD1 were analyzed via the *Analyze Area Fraction* function.

2.7. $Ca_V2.2$ detection in human ALS brain samples

Human spinal cord (n_{ALS} = 3, n_{CON} = 5, 6♂:2♀) and medulla oblongata (n_{ALS} = 4, n_{CON} = 4, 4♂:4♀) paraffin-embedded tissues samples were obtained from The Netherlands Brain Bank, Netherlands Institute for Neuroscience, Amsterdam (NBB, open access: www.brainbank.nl). Because these were the only spinal cord samples available at the NBB, a balanced gender distribution was not possible. Tissue sections (10 µm thickness) were prepared using a microtome (Mikrom HM 355S, Thermo Fisher Scientific Inc., USA). Sections were used to detect $Ca_V2.2$ expression and to compare signal intensity between ALS-diagnosed patients and non-demented control individuals (CON).

Slices were deparaffinized using ROTI®Histol (Carl Roth GmbH + Co. KG, Karlsruhe, Germany) and ethanol. Antigen retrieval was then performed with 1 mM EDTA (pH 8) buffer. Next, sections were incubated with the primary antibody rabbit-anti-$Ca_V2.2$ (Alomone Labs, Jerusalem, Israel) over night at 4 °C (1:500). On the following day, the secondary antibody was incubated for 2 h at room temperature. Quantification of $Ca_V2.2$ staining was performed using ImageJ with the *Analyze Area Fraction* and *Analyze Particles* function as described above.

2.8. Statistics

First, differences between part 1 and part 2 of the study were analyzed by three-way ANOVA (factors: genotype x age x part). If a significant three-way interaction was detected, subsequent simple main effect tests were performed, followed by post-hoc Holm-Sidak tests. Significant results are displayed in the corresponding tables. If no significant three-way interaction was detected, a subsequent two-way ANOVA (factors: part × genotype, and part × age) was performed. When significant differences were detected, post-hoc Holm-Sidak tests were conducted to determine the influence of the different parts on genotype or age, which is displayed in the corresponding tables. The same procedure was applied to evaluate potential sex-dependent differences. This manuscript does not include details for the three-way and two-way ANOVAs performed for the influence of factors part and sex.

Second, weekly tests, body weight, and OFT were analyzed using two-way repeated measures (RM) ANOVA (factors: genotype x age) followed by post-hoc Holm-Sidak tests. Results of the post-hoc tests are displayed in the corresponding tables. Disease onset and survival were analyzed using Kaplan-Meyer survival analysis with log-rank testing. Quantitative histological data were analyzed using one-way ANOVA and post-hoc Holm-Sidak tests for parametric data. The second analyses focused on the influence of the $Ca_V2.2$ KO on the performance of the mice. Details for these statistical tests are displayed in the figure captions and in the tables that present the post-hoc tests.

Statistical significance was defined as $p < 0.05$. All statistical analyses were performed with Sigma Plot v.11.0 (Systat Software, Erkrath, Germany). Data were visualized using GraphPad PRISM v.5.00 (GraphPad Software, Inc., La Jolla, CA, USA).

3. Results

3.1. Breeding of $Cav^{-/-}$-SOD1 mice revealed a non-mendelian inheritance

The generation of mice was expected to follow Mendel's rules of inheritance. Accordingly, breeding male $Cav^{+/-}$-SOD1 and female $Cav^{+/-}$ mice should yield 12.5% of the offspring with the desired $Cav^{-/-}$-SOD1 genotype. However, only 6.6% of the offspring obtained carried the $Cav^{-/-}$-SOD1 genotype. Thus, a second cohort was generated because the number of mice with the desired genotype was insufficient. In the breeding strategy for the second part of the study, the observed genotype distribution from the first cohort was used (Table 1, part 1). The genotype distribution in the second cohort confirmed the non-mendelian inheritance pattern with only 6.2% of the progeny exhibiting the desired $Cav^{-/-}$-SOD1 genotype (Table 1, part 2). Importantly, this phenomenon only occurred when crossing $Cav^{+/-}$-SOD1 with $Cav^{+/-}$ mice, but not observed when SOD1 mice were crossed with $Cav^{+/-}$ mice. Overall, the mean litter size was 6.5 pups per litter, and the mean loss before weaning was 12.7% independent of genotype.

Notably, five of the nine $Cav^{-/-}$ mice participating in the second part of the study suffered seizures. Three of these five mice had to be sacrificed as they reached termination criteria in a health check after they did not recover from a seizure. Additionally, from eight $Cav^{-/-}$-SOD1 mice in the second part, five mice had seizures (under 1 min, fast recovery). None of these $Cav^{-/-}$-SOD1 animals reached a critical health status because of a seizure. This phenotype was not visible in the first part of the study.

3.2. $Cav^{-/-}$-SOD1 mice show no weight difference to SOD1 mice

During the study period, mice were weighed three times per week. Two mice were excluded from weight analysis because of the presence of elephant tooth, and three additional mice were excluded because of health issues that caused weight fluctuations. The mean body weight per week is shown in Fig. 1 A. WT and $Cav^{-/-}$ mice showed comparable increases in body weight over time, whereas $Cav^{-/-}$ mice showed lower weights than WT mice, particularly during the initial weeks; however, this difference was not statistically significant (Table 2). A similar pattern was observed for SOD1 and $Cav^{-/-}$-SOD1 mice, which exhibited three distinct phases: an initial phase of weight gain, followed by weight stagnation, and finally a phase of weight loss. Overall, the $Cav^{-/-}$-SOD1 mice weighed less than the SOD1 mice throughout most of the study period (non-significant, Table 2). Additionally, female mice weighed significantly less than male mice across the whole study period independent of genotypes (Fig. 1 C, E, G, I, Table 2).

$Cav^{-/-}$ and $Cav^{-/-}$-SOD1 mice showed a steeper increase during the first weeks compared with WT and SOD1 mice, respectively, when relative weight change was analyzed (Fig. 1 B). This resulted in a significantly greater weight change over several weeks (Table 2). Both,

Table 1
Non-mendelian inheritance of the $Cav^{-/-}$-SOD1 genotype.

	$Cav^{-/-}$-SOD1	$Cav^{+/-}$-SOD1	SOD1	$Cav^{-/-}$	$Cav^{+/-}$	WT
expected [%]	12.5	25	12.5	12.5	25	12.5
part 1 [%]	6.6	22.3	11.6	12.4	26.4	20.7
part 2 [%]	5.9	30.1	7.5	11.8	33.4	11.3
combined [%]	6.2	26.2	9.6	12.1	29.9	16.0

The first part of the breeding strategy did not meet the necessary animal number to perform the study as the $Cav^{-/-}$-SOD1 genotype is not distributed according to mendelian inheritance. The same phenomenon occurred in the second part of the study. To summarize, cross-breeding the $Ca_V2.2$ KO mice with the SOD1*G93A mice resulted in only half of the estimated number of double-transgenic $Cav^{-/-}$-SOD1 mice.

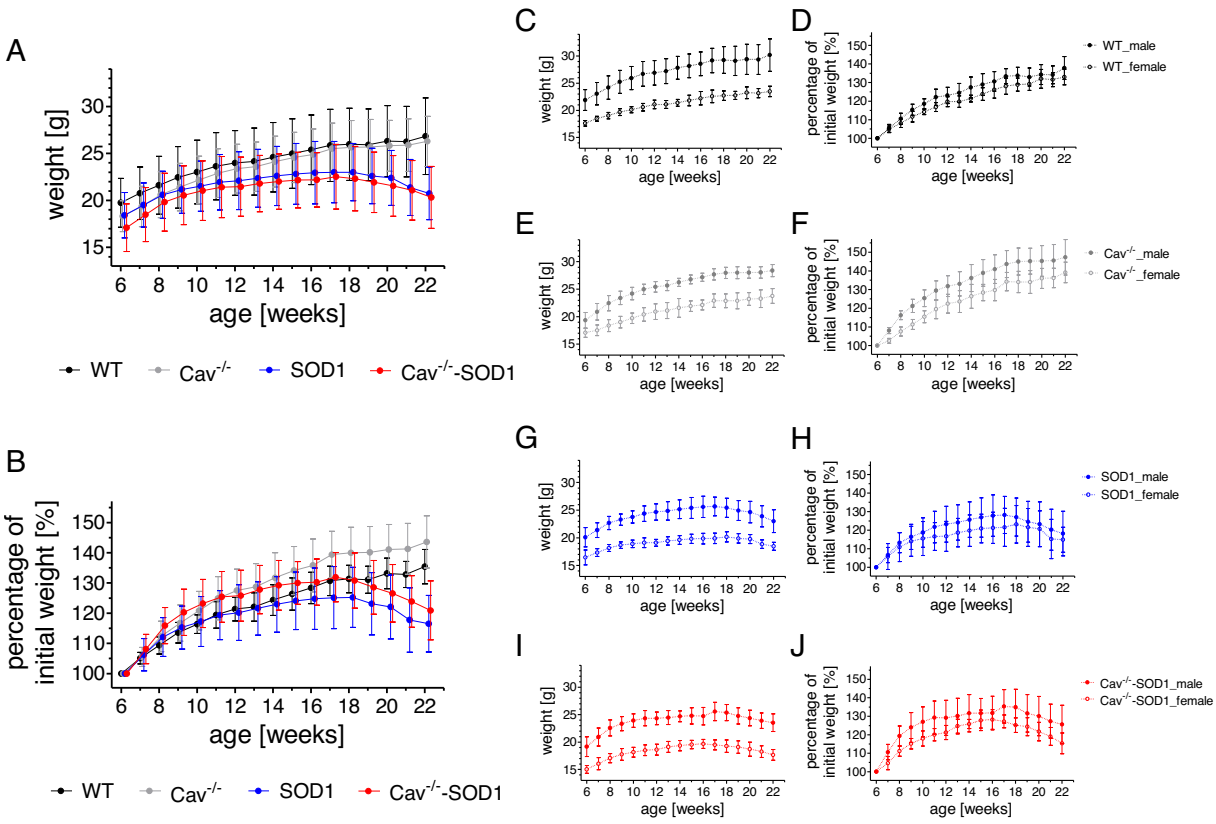

Fig. 1. Total weight and weight change.
(A–B) Data shown are the averages (mean ± SD) of weight measurements taken three-times per week. WT and Cav$^{-/-}$ mice showed a steady weight gain whereas the weight of SOD1 and Cav$^{-/-}$-SOD1 mice first stagnated and then decreased. Statistical analysis was performed using two-way RM ANOVA for the effect of genotype and age on total weight and percentage of weight change. (A) $F_{interaction}(54,44) = 20.778$, $p < 0.001$; $F_{genotype}(3, 44) = 4.168$, $p = 0.011$; $F_{age}(18, 44) = 250.758$, $p < 0.001$; (B) $F_{interaction}(54,44) = 20.202$, $p < 0.001$; $F_{genotype}(3, 44) = 7.013$, $p < 0.001$; $F_{age}(18, 44) = 262.691$, $p < 0.001$. (C–J) Weight differences between the sexes are separately depicted for each genotype (mean ± SD). Statistical differences were detected using two-way ANOVA (factors: sex x age) and post-hoc Holm-Sidak tests for each genotype. (A–J) WT (n = 13, 6♂:7♀), Cav$^{-/-}$ (n = 11, 6♂:5♀), SOD1 (n = 13, 7♂:6♀), Cav$^{-/-}$-SOD1 (n = 13, 7♂:6♀).

Table 2
Holm-Sidak tests for the total body weight and weight change.

genotype differences	WT vs. SOD1	WT vs. Cav$^{-/-}$-SOD1	SOD1 vs. Cav$^{-/-}$-SOD1	Cav$^{-/-}$ vs. WT
total weight	19–22	18–22	ns	ns
weight change	19–22	21–22	21	17–22

sex differences	WT	Cav$^{-/-}$	WT	Cav$^{-/-}$-SOD1
total weight	6–22	6–22	6–22	6–22
weight change	11, 13–15, 17–18, 22	6–22	ns	ns

After two-way RM ANOVA, post-hoc Holm-Sidak tests were performed to test for differences between the genotypes (WT, Cav$^{-/-}$, SOD1, Cav$^{-/-}$-SOD1) at different ages. Sex differences (male vs. female) at different ages were analyzed using two-way ANOVA and post-hoc Holm-Sidak tests for each genotype. The significant weeks ($p < 0.05$) during the study period are shown for the total weight and weight change. ns = non-significant.

SOD1 and Cav$^{-/-}$-SOD1 mice lost weight significantly compared with WT mice from week 18 till week 22 (Table 2). The overall weight change was comparable between Cav$^{-/-}$ and WT, and Cav$^{-/-}$-SOD1 and SOD1 mice. When comparing the sexes, only Cav$^{-/-}$ mice showed significant differences throughout the study period. In WT mice, sex-related differences were observed only during few weeks, whereas no significant sex differences in weight change were detected for Cav$^{-/-}$-SOD1 and SOD1 mice (Table 2).

3.3. *Cav$^{-/-}$-SOD1 mice show improved motor functions*

ALS-like phenotype progression was assessed using the SHIRPA and splay reflex test. Cav$^{-/-}$ mice did not differ from WT mice in the SHIRPA score sum (Fig. 1 A) or the motor score sum (Fig. 1 B), which was confirmed by two-way RM ANOVA followed by Holm-Sidak post-hoc testing. In contrast, SOD1 and Cav$^{-/-}$-SOD1 mice displayed significantly elevated score sums from approximately 11 weeks of age onwards. Importantly, Cav$^{-/-}$-SOD1 mice showed a slightly but significantly reduced phenotype severity in the SHIRPA score and the motor score compared with SOD1 mice from week 15 until the end of the study period (Table 3).

Cav$^{-/-}$-SOD1 mice exhibited significantly improved splay score sums compared with SOD1 mice between weeks 8 to 20. Cav$^{-/-}$-SOD1 mice did not differ significantly from WT mice until 15 weeks of age. In contrast, SOD1 mice showed significantly elevated splay score sums starting at 8 weeks of age. As observed for the SHIRPA assessment, Cav$^{-/-}$ mice did not differ from WT mice (Table 3). The splay reflex test revealed significant differences between parts 1 and 2 of the study at weeks 11, 19, and 20 (three-way ANOVA followed by Holm-Sidak post-hoc testing). However, because this effect was not consistent throughout the entire study period, comparisons between age and genotype on the splay score sum remain interpretable (Table 3).

Table 3
Holm-Sidak tests for the SHIRPA test, motor score of the SHIRPA test, and splay reflex test.

genotype differences	WT vs. SOD1	WT vs. $Cav^{-/-}$-SOD1	SOD1 vs. $Cav^{-/-}$-SOD1	$Cav^{-/-}$ vs. WT
SHIRPA score sum, SHIRPA test	11–21	11–21	15–21	ns
motor score sum, SHIRPA test	13–21	14–21	15–19	ns
splay score sum, splay reflex test	8, 10–21	16–21	8–20	ns

part differences	averaged over levels of genotype
splay score sum, splay reflex test	11, 19–20

After two-way RM ANOVA, post-hoc Holm-Sidak tests were performed to test for differences between the genotypes (WT, $Cav^{-/-}$, SOD1, $Cav^{-/-}$-SOD1) at different ages. Sex differences (male vs. female) at different ages and averaged over levels of genotype were analyzed using three-way ANOVA and post-hoc Holm-Sidak tests. The significant weeks ($p < 0.05$) during the study period are shown for the SHIRPA score sum, motor score sum, and splay score sum. ns = non-significant.

3.4. The additive effect of the $Ca_V2.2$ channel KO

In the OFT, four parameters were analyzed: distance moved, time spent moving, and exploration of the center and border zones. For the first two parameters (Fig. 3 A–B), $Cav^{-/-}$ mice showed significantly greater locomotor activity than WT mice across all four test rounds. This increased activity was also observed in $Cav^{-/-}$-SOD1 mice, which was significant compared with WT and SOD1 mice in all OFT rounds. In contrast, WT and SOD1 mice did not differ significantly, except for a single difference observed at week 18 (Table 4). The results for distance moved and time spent moving also revealed sex-dependent differences within the $Cav^{-/-}$ group (distance moved: week 10, time spent moving: 6 and 18 weeks; Table 4). These observations suggest that the increased mobility of $Cav^{-/-}$ mice may be more pronounced in female $Cav^{-/-}$ mice. Moreover, on week 14 the difference between parts 1 and 2 within the SOD1 group was significant (Table 4). Two-way RM ANOVA did not reveal significant main effects of genotype or age for border or center exploration (Fig. 3 C-D).

During the pole test (Fig. 3 E), $Cav^{-/-}$ mice exhibited progressively increasing pole score sums, reflecting a behavior characterized by stumbling and sliding off the pole rather than controlled locomotion. This behavior yielded significantly higher pole score sums during most of the study period (Table 4), and was partly observed in $Cav^{-/-}$-SOD1 mice leading to poorer performance in the pole test compared with SOD1 mice, which became significant in weeks 18 and 19 (Table 4). Thus, $Cav^{-/-}$-SOD1 mice appear to combine the motor deficits associated with the SOD1 genotype with a potential coordination deficit observed in $Cav^{-/-}$ mice, resulting in a deterioration of pole test performance compared with SOD1 mice.

A similar effect was observed in the hanging wire test. In the first part of the study (Fig. 3 F), $Cav^{-/-}$ mice showed a shorter latency to fall compared with WT mice. Their behavior appeared to involve voluntary jumping from the grid rather than falling because of muscle weakness. Nevertheless, this difference was statistically significant, particularly during the early weeks of the study (Table 4). $Cav^{-/-}$-SOD1 mice performed worse than SOD1 mice, reaching significance in the weeks preceding disease onset, i.e., before week 15 (Table 4). In the second part of the study, the hanging wire test was modified from a single 300 s interval to three consecutive 100 s intervals (Fig. 3 G). This modification reduced the jumping behavior of the $Cav^{-/-}$ mice resulting in a performance comparable to WT mice. Interestingly, the difference between the $Cav^{-/-}$-SOD1 and SOD1 mice persisted in the modified version, with $Cav^{-/-}$-SOD1 mice still showing reduced latencies to fall from week 10 to week 18. Although SOD1 mice displayed a significant reduction in latency to fall around disease onset, $Cav^{-/-}$-SOD1 mice showed reduced latencies beginning after week 9 compared with WT mice (Table 4).

Table 4
Holm-Sidak tests for the OFT, pole test, and hanging wire test.

genotype differences	WT vs. SOD1	WT vs. $Cav^{-/-}$-SOD1	SOD1 vs. $Cav^{-/-}$-SOD1	$Cav^{-/-}$ vs. WT
distance moved, OFT	ns	6, 10, 14, 18	6, 10, 14, 18	6, 10, 14, 18
time spent moving, OFT	ns	6, 10, 14, 18	6, 10, 14, 18	6, 10, 14, 18
pole score sum, pole test	14–20	12–20	18–19	12, 14–20
latency to fall, hanging wire, part 1	8–20	6–20	6–8, 10, 14	6–9, 14
latency to fall, hanging wire, part 2	15–20	10–20	10, 12–18	14

sex differences	WT	$Cav^{-/-}$	SOD1	$Cav^{-/-}$-SOD1
distance moved, OFT	ns	10	ns	ns
time spent moving, OFT	ns	6, 18	ns	ns
pole score sum, pole test	ns	ns	14–16, 20	13–20
latency to fall, hanging wire, part 1	9, 19	11, 16	ns	7

part differences	WT	$Cav^{-/-}$	SOD1	$Cav^{-/-}$-SOD1
time spent moving, OFT	ns	ns	14	ns
pole score sum, pole test	19	11, 14	ns	ns

After two-way RM ANOVA, post-hoc Holm-Sidak tests were performed to test for differences between the genotypes (WT, $Cav^{-/-}$, SOD1, $Cav^{-/-}$-SOD1) at different ages. Sex differences (male vs. female) and part differences (part 1 vs. part 2) at different ages were analyzed using two-way ANOVA and post-hoc Holm-Sidak tests for each genotype. The significant weeks ($p < 0.05$) during the study period are shown for the distance moved (OFT), time spent moving (OFT), pole score sum, latency to fall in part 1 (hanging wire), and latency to fall in part 2 (hanging wire). ns = non-significant.

3.5. Studying the non-WT-like behavior of $Cav^{-/-}$ mice

As $Cav^{-/-}$ mice displayed behavioral differences compared with WT mice during the first part of the study, additional behavioral tests were performed in the second part. In the first part, OFT data revealed increased locomotor activity in $Cav^{-/-}$ mice, as indicated by a greater distance moved and longer time spent moving, whereas border and center exploration did not differ between genotypes (Fig. 3 A–D). To determine whether exploratory behavior toward novel stimuli differed between genotypes, an object exploration test was performed by placing an object in the center of the arena (Fig. 4 A–D). $Cav^{-/-}$ mice again exhibited an increased distance moved and longer time spent moving (Fig. 4 A–B), similar to the observations in the OFT, and these differences

were significant in all tested weeks. Cav$^{-/-}$-SOD1 mice also showed increased locomotor activity compared with WT and SOD1 mice during several test weeks (Table 5), verifying the findings from the OFT. Analysis of sex differences within the Cav$^{-/-}$-SOD1 group revealed significant differences in distance moved and time spent moving (distance moved: 10 and 14 weeks, time spent moving: week 10; Table 5). In Cav$^{-/-}$ mice, a single significant sex difference was detected at week 18 (Table 5). Introducing an object into the center of the arena, WT mice spent less than 100 s exploring the object, whereas all other genotypes exceeded 100 s of exploratory time (Fig. 4 C-D). In particular, Cav$^{-/-}$-SOD1 and Cav$^{-/-}$ mice spent significantly more time exploring the object than WT and SOD1 mice (Table 5).

In the hanging wire test and pole test, Cav$^{-/-}$ mice partially performed worse than WT mice (Fig. 3 E–G). To test the muscle strength and motor coordination in Cav$^{-/-}$ mice, the grip strength test and rotarod test were included in part 2 of the study. Peak forces were similar between Cav$^{-/-}$ and WT mice, and between Cav$^{-/-}$-SOD1 and SOD1 mice (Fig. 4 E). However, significant losses of grip strength were observed in SOD1 mice at disease onset, and even earlier in Cav$^{-/-}$-SOD1 mice compared with WT mice (Table 5). Similar trends were observed for the rotarod test (Fig. 4 F). WT and Cav$^{-/-}$ mice showed similar latencies to fall, whereas Cav$^{-/-}$-SOD1 and SOD1 mice exhibited similarly reduced latencies. Over time, SOD1 and Cav$^{-/-}$-SOD1 mice showed progressively poorer rotarod performance, which became statistically significant from the second testing round onward (Table 5).

Additionally, Cav$^{-/-}$ mice were repeatedly observed running and jumping in the experimental cages during resting phases between tests. Similar behavior was occasionally observed in some Cav$^{-/-}$-SOD1 mice.

Table 5
Holm-Sidak tests for the object exploration test, grip strength test, rotarod test, and gnawing analysis.

genotype differences				
	WT vs. SOD1	WT vs. Cav$^{-/-}$-SOD1	SOD1 vs. Cav$^{-/-}$-SOD1	Cav$^{-/-}$ vs. WT
distance moved, object exploration	ns	ns	ns	6, 10, 14, 18
time spent moving, object exploration	ns	6, 18	ns	6, 10, 18
border exploration, object exploration	ns	6, 10, 14, 18	6, 18	6, 10, 14, 18
center exploration, object exploration	ns	6, 10, 14, 18	6, 18	6, 10, 14, 18
peak force, grip strength	16–20	6, 10, 14–20	ns	ns
latency to fall, rotarod	15, 19	11, 15, 19	ns	7
left tissue, gnawing analysis	ns	ns	ns	12–14

sex differences				
	WT	Cav$^{-/-}$	SOD1	Cav$^{-/-}$-SOD1
distance moved, object exploration	ns	18	ns	10, 14
time spent moving, object exploration	ns	ns	ns	10
left tissue, gnawing analysis	ns	9, 11–13	9, 12, 16–17	ns

After two-way RM ANOVA, post-hoc Holm-Sidak tests were performed to test for differences between the genotypes (WT, Cav$^{-/-}$, SOD1, Cav$^{-/-}$-SOD1) at different ages. Sex differences (male vs. female) at different ages were analyzed using two-way ANOVA and post-hoc Holm-Sidak tests for each genotype. The significant weeks ($p < 0.05$) during the study period are shown for the distance moved (object exploration test), time spent moving (object exploration test), border exploration time (object exploration test), center exploration time (object exploration test), peak force (grip strength test), latency to fall (rotarod test), and left tissue area (gnawing analysis). ns = non-significant.

To quantify this activity, paper tissues were placed in the cages and evaluated for gnawing activity (Fig. 4 G). Cav$^{-/-}$ mice gnawed on the paper tissue considerably more than WT mice throughout the study period, which was significant between weeks 12 and 14. No differences in the remaining tissue area were observed between the other genotypes (Table 5). Evaluation of sex-dependent differences in gnawing behavior revealed significant differences in Cav$^{-/-}$ and SOD1 mice (Table 5).

3.6. Knockout of the $Ca_V2.2$ channel delays disease onset but does not prolong survival in SOD1*G93A mice

Disease onset has been defined previously as the first day on which tremor in the hind limbs and a reduced splay reflex in at least one limb occurred simultaneously (Mead et al., 2011). At this time point, the onset score was changed from 0 to 1. Cav$^{-/-}$-SOD1 mice displayed a delayed disease onset ($p < 0.001$) with a median age at onset of 125 days compared with 107 days for SOD1 mice (Fig. 5 A). The beneficial effect of the $Ca_v2.2$ knockout was not reflected in overall survival (Fig. 5 B). Cav$^{-/-}$-SOD1 mice did not exhibit prolonged survival compared to SOD1 mice (Cav$^{-/-}$-SOD1 165 days vs. SOD1 162 days, $p = 0.274$). WT and Cav$^{-/-}$ mice did not develop the ALS-like phenotypes (e.g., tremor, splay deficit) during the observation period.

3.7. Knockout of the $Ca_V2.2$ channel does not rescue neurons or reduce inflammation but reduces aggregation of SOD1 protein

Histological analysis of the spinal cord at end stage was performed using markers for activated astrocytes (GFAP), activated microglia (Iba1), neuronal nuclei (NeuN), and motor neurons (ChAT). NeuN and ChAT cell counts and the area fractions of GFAP and Iba1 signals were compared between genotypes in the ventral horn (Fig. 6 A–D; Supplement Figs. 1 and 2). No significant differences were observed between WT and Cav$^{-/-}$ mice or SOD1 and Cav$^{-/-}$-SOD1 mice. In general, neuronal markers were significantly reduced (NeuN: WT 175.60 ± 4.53 and Cav$^{-/-}$ 178.63 ± 6.27 vs. SOD1 116.94 ± 8.83 and Cav$^{-/-}$-SOD1 119.43 ± 11.12; ChAT: WT 13.45 ± 0.63 and Cav$^{-/-}$ 12.70 ± 0.63 vs. SOD1 6.23 ± 0.23 and Cav$^{-/-}$-SOD1 6.61 ± 0.45), while inflammatory markers were significantly increased (GFAP: WT 8.43% ± 0.62% and Cav$^{-/-}$ 6.53% ± 0.98% vs. SOD1 29.47% ± 1.68% and Cav$^{-/-}$-SOD1 27.28% ± 2.56%; Iba1: WT 2.83% ± 0.73% and Cav$^{-/-}$ 3.68% ± 0.78% vs. SOD1 10.03% ± 0.99% and Cav$^{-/-}$-SOD1 9.61% ± 1.61%) in SOD1 and Cav$^{-/-}$-SOD1 mice compared to WT and Cav$^{-/-}$ mice ($p < 0.001$).

The same analysis was performed in the pons region of the brain, specifically within the trigeminal motor nucleus (Fig. 6 F–I; Supplement Figs. 3 and 4). Neuronal markers were downregulated in Cav$^{-/-}$-SOD1 and SOD1 mice, but these differences did not reach statistical significance. In contrast, Iba1 and GFAP were significantly increased ($p < 0.001$) in SOD1 and Cav$^{-/-}$-SOD1 mice. Again, there were no differences between WT and Cav$^{-/-}$ mice (GFAP: 0.51% ± 0.09% and 0.86% ± 0.22%; Iba1: 1.80% ± 0.28% and 1.92% ± 0.16%), and SOD1 and Cav$^{-/-}$-SOD1 mice (GFAP: 7.21% ± 0.62% and 7.92% ± 0.80%; Iba1: 6.85% ± 3.40% and 6.89% ± 0.73%).

In the medulla oblongata, specifically in the facial motor nucleus (Fig. 6 K–N; Supplement Figs. 5 and 6), NeuN and ChAT cell counts were not significantly reduced in SOD1 or Cav$^{-/-}$-SOD1 mice compared with WT mice. GFAP signals were slightly elevated in Cav$^{-/-}$-SOD1 mice; although this did not reach statistical significance. Only SOD1 mice (3.70% ± 1.10%) showed a significantly increased GFAP signal compared with WT (0.39% ± 0.08%) and Cav$^{-/-}$ (0.41% ± 0.16%) mice. SOD1 and Cav$^{-/-}$-SOD1 mice exhibited significantly elevated Iba1 signals compared with WT and Cav$^{-/-}$ mice. Additionally, Cav$^{-/-}$-SOD1 mice displayed a higher number of Iba1-positive cells compared with SOD1 mice (7.33% ± 0.64% vs. 5.92% ± 0.32%, $p < 0.005$).

Tissue sections from the spinal cord (Fig. 6 E, Supplement Fig. 8), pons (Fig. 6 J, Supplement Fig. 9), and medulla oblongata (Fig. 6 O,

Supplement Fig. 10) were stained for accumulated SOD1 protein aggregates. In all regions, Cav$^{-/-}$-SOD1 mice exhibited reduced SOD1 aggregation compared with SOD1 mice. In the brain regions analyzed, reduction reached statistical significance (pons: SOD1 14.71% ± 1.75% vs. Cav$^{-/-}$-SOD1 9.39% ± 0.74%, $p < 0.001$; medulla: SOD1 5.88% ± 0.62% vs. Cav$^{-/-}$-SOD1 4.26% ± 0.44%, $p < 0.05$). WT and Cav$^{-/-}$ mice did not exhibit detectable SOD1 aggregation.

3.8. Detection of the $Ca_V2.2$ calcium channel in human ALS samples

The importance of the $Ca_V2.2$ channel in human ALS patients was investigated using post-mortem tissue samples obtained from the Netherlands Brain Bank. Spinal cord tissue from six individuals and medulla oblongata tissues from eight individuals were analyzed (Table 6). The uneven gender distribution and discrepancies in mean age between ALS and control groups reflects the limited availability of suitable samples and the typical earlier death of ALS patients. All samples were sectioned using a microtome and underwent immunofluorescence staining with a $Ca_V2.2$-specific antibody.

Histological analysis confirmed the presence of $Ca_V2.2$ immunoreactivity in tissue from control and ALS-diagnosed patients. In the medulla oblongata (Fig. 7 A–D), a greater number of cells displayed $Ca_V2.2$ staining compared with the spinal cord (Fig. 7 E–H). Moreover, the staining intensity appeared stronger in ALS samples than in control tissue. Quantitative analysis of fluorescence intensity in the medulla oblongata and spinal cord revealed higher $Ca_V2.2$ signal levels in ALS patients (Fig. 7 I–J). Statistical analysis using a *t*-test indicated significant differences in the medulla oblongata ($p = 0.027$) and spinal cord ($p = 0.039$), suggesting a potential involvement of the N-type channel in ALS disease pathology and progression.

4. Discussion

Amyotrophic lateral sclerosis is a fatal motor neuron disease of largely unknown etiology with limited therapeutic options. The multifactorial nature of ALS complicates therapeutic intervention, as multiple disease-driving mechanisms must be targeted simultaneously. Therefore, identifying new treatments remains a priority. RD2RD2, a new drug candidate belonging to the class of all-D-enantiomeric peptides, has previously shown efficacy in the early stages of disease in SOD1*G93A mice (Post et al., 2021a; Post et al., 2021b; Wintz et al., 2023). In vitro, RD2RD2 inhibited the $Ca_V2.2$ voltage-gated calcium channel (VGCC), which plays an important role in neurotransmitter release and glial regulation (Huntula et al., 2019; Jurkovicova-Tarabova and Lacinova, 2019). Although less potent than the specific N-type channel inhibitor ω-conotoxin GVIA, RD2RD2 markedly reduced binding of radiolabeled GVIA (i.e., $IC_{50} = 20$ nM, $K_i = 16.9$ nM; data not shown). Notably, $Ca_V2.2$ is overexpressed in isolated SOD1*G93A neurons (Pieri et al., 2013) and is associated with increased motor neuron firing (Chang and Martin, 2016). By generating $Ca_V2.2$-deficient SOD1 mice through crossing the SOD1*G93A ALS mouse line with the Cacna1b KO mouse line, we were able to characterize the role of this N-type channel in ALS pathology.

A non-mendelian inheritance was observed for the Cav$^{-/-}$-SOD1 genotype (Table 1), likely reflecting the increased mortality rate at weaning; however, genotyping was not possible for the affected mice because of maternal cannibalism. Elevated pre-weaning mortality has also been reported in Cav$^{-/-}$ mice (~30%) (Saegusa et al., 2001). In this study, the Cav$^{-/-}$ genotype did not show increased mortality (Table 1). Overall, the N-type channel might play a role in embryogenic or early postnatal development.

Behaviorally, Cav$^{-/-}$ mice differed markedly from WT mice in this study. Saegusa et al. described the mice as having a reduced anxiety-linked behavior and reduced inflammatory and neuropathic pain perception (Saegusa et al., 2001). In the modified pole and hanging wire test, Cav$^{-/-}$ (Fig. 4 E) mice showed elevated pole score sums and reduced latency to fall (Fig. 3 E–F). However, grip strength testing revealed no differences in hind limb force (Fig. 4 E). Rather, mice appeared to voluntarily release from the grid. This behavior was eliminated by modifying the test to use repeated 100 s trials (Fig. 3 G). Similarly, rotarod testing showed no deficits in motor coordination (Fig. 4 F), suggesting that the elevated pole score sums were not caused by motor dysfunction.

Elevated pole score sums may reflect rapid and imprecise movements of Cav$^{-/-}$ mice. The mice showed an increased distance moved and time spent moving (Fig. 3 A–D), resulting in higher velocity, consistent with reduced anxiety reported previously (Saegusa et al., 2001). This increased activity likely contributed to inaccurate limb placement during the pole test. Similar hyperactivity was also observed in the experimental cages, where Cav$^{-/-}$ mice repeatedly ran or jumped. Enhanced gnawing behavior (Fig. 4 G), a known stereotypy (Würbel et al., 1998), further supports this interpretation and may be compensatory in contrast to running and jumping. Overall, $Ca_V2.2$ deficiency induces a hyperactive or stereotypic phenotype, potentially relevant to obsessive-compulsive spectrum disorders (Ting and Feng, 2008; Xiao et al., 2025).

When an object was introduced into the OFT arena, Cav$^{-/-}$ mice showed significantly increased exploration (Fig. 4 A–D). This observation suggested reduced anxiety, increased exploratory behavior, or both, although long-term memory impairment may also contribute, as reported in a passive avoidance test with a similar $Ca_V2.2$ KO mouse model (Nakagawasai et al., 2010).

The most striking observation for the Cav$^{-/-}$ phenotype was that some mice in part 2 had seizures. Bi-allelic loss-of-function mutations in *CACNA1B* are associated with early-onset epileptic seizures with involuntary hyperkinetic movement disorders in children (Gorman et al., 2019). Given the role of $Ca_V2.2$ in presynaptic vesicle fusion, its absence may disrupt neurotransmission and promote seizure activity. Consistent with this, other synaptic proteins (e.g., synapsin 1, syntaxin-binding protein 1) are associated with monogenic epilepsies (Jiang et al., 2025). Mouse models with $Ca_V2.2$ KO are therefore also a potential epilepsy model. Additional phenotypes reported in N-type-deficient models include hyperactivity, vigilance state differences (Beuckmann et al., 2003), and impaired sympathetic regulation of the circulatory system (Mori et al., 2002). Importantly, $Ca_V2.2$ function cannot be fully compensated by other VGCCs of the Ca_V2 family ($Ca_V2.1$ P/Q-type; $Ca_V2.3$ L-type) (Hatakeyama et al., 2001; Ino et al., 2001), despite partial developmental replacement by $Ca_V2.1$ channels (Iwasaki et al., 2000), further highlighting its critical role in early neuronal development.

In SOD1*G93A mice, $Ca_V2.2$ KO reduced disease severity in early stages, as indicated by the improved SHIRPA score sum, SHIRPA motor score sum, and splay score sum (Fig. 2, Table 3). However, the effect diminished over time (i.e., similar in the last test weeks), suggesting a preliminary early impact on disease progression. This result aligns with our previous RD2RD2 studies, which showed transient efficacy until ~ 21 weeks (Wintz et al., 2023) supporting the notion that both approaches target similar $Ca_V2.2$-related mechanisms. Additionally, our previous studies showed a reduced pole score sum after RD2RD2 treatment (Post et al., 2021b; Wintz et al., 2023). Here, we cannot reproduce these results as the N-type KO had a negative effect on the pole performance in Cav$^{-/-}$-SOD1 mice (Fig. 3 E). It remains unclear if these elevated score sums were the result of a combination of the SOD1

Table 6
Overview of human tissue samples.

samples	spinal cord (n)	medulla oblongata (n)	sex	mean age [years]
ALS	3	4	5♂:2♀	62.7
CON	5	4	5♂:4♀	80.6

Human, paraffin-embedded tissue was obtained from the Netherlands Brain Bank (Amsterdam, Netherlands). Control (CON) samples and samples from ALS-diagnosed patients included tissue from the spinal cord and medulla oblongata.

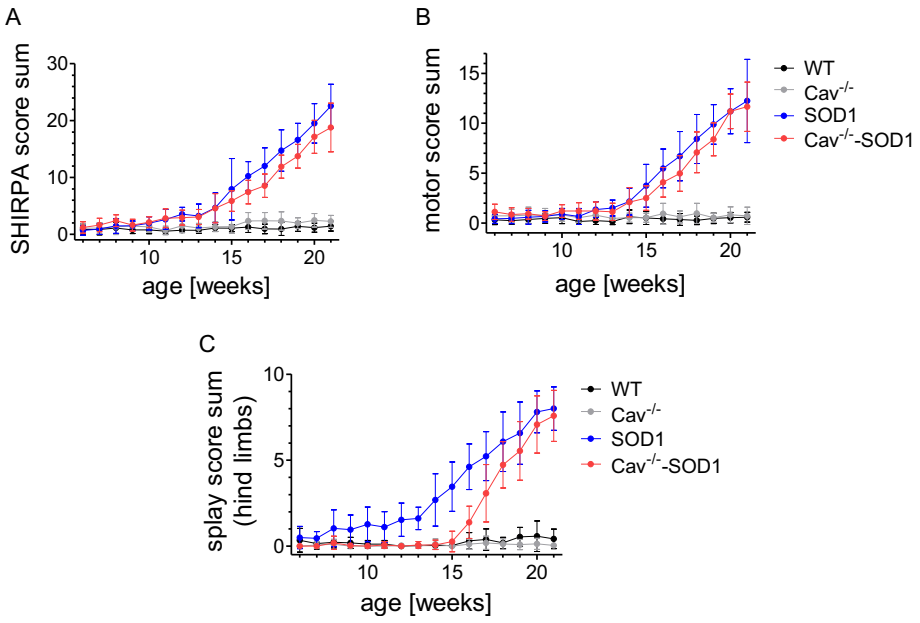

Fig. 2. $Cav^{-/-}$-SOD1 mice show improved motor functions.
$Cav^{-/-}$-SOD1 mice showed improved SHIRPA score sums (A), motor score sums (B) and splay score sums (C) in comparison to SOD1 mice. Data presented are the mean ± SD. Statistical analysis was performed using two-way RM ANOVA for the effect of genotype and age on each score sum. (A) $F_{interaction}(45,49) = 63.760$, $p < 0.001$; $F_{genotype}(3,49) = 190.562$, $p < 0.001$; $F_{age}(15,49) = 224.862$, $p < 0.001$; (B) $F_{interaction}(45,49) = 58.838$, $p < 0.001$; $F_{genotype}(3,49) = 171.2215$, $p < 0.001$; $F_{age}(15,49) = 180.544$, $p < 0.001$; (C) $F_{interaction}(45,49) = 59.278$, $p < 0.001$; $F_{genotype}(3,49) = 195.313$, $p < 0.001$; $F_{age}(15,49) = 188.738$, $p < 0.001$. (A–C) WT (n = 14, 7♂:7♀), $Cav^{-/-}$ (n = 14, 7♂:7♀), SOD1 (n = 13, 7♂:6♀), $Cav^{-/-}$-SOD1 (n = 14, 8♂:6♀).

motoric phenotype and the $Cav^{-/-}$ coordinative phenotype. Thus, the interpretation of pole results in this model is limited, and alternative protocols may improve discrimination, such as placing mice head-upward on the pole requiring them to invert to descend to the ground (Matsuura et al., 1997).

In the hanging wire test, protocol modification improved interpretability. Although $Cav^{-/-}$ mice showed a worse performance than WT mice, shortening the test interval resulted in $Cav^{-/-}$ mice performing as WT-like. However, the performance of $Cav^{-/-}$-SOD1 mice remained impaired (Fig. 3 F-G), suggesting a deficit in sustained muscle performance. This result contrasts with RD2RD2 studies (Wintz et al., 2023), possibly reflecting incomplete pharmacological inhibition relative to complete genetic ablation. Notably, differences diminished over time, reinforcing the early effect of $Ca_V2.2$ deficiency. Grip strength and rotarod tests did not reveal differences between $Cav^{-/-}$-SOD1 and SOD1 mice (Fig. 4 E–F, Table 5), indicating that deficits because of N-type KO are specific to prolonged exertion (i.e., grip strength: few seconds; hanging wire test: 100 s). Although exploratory behavior in an empty arena for $Cav^{-/-}$-SOD1 mice was unchanged compared with WT and SOD1 mice (Fig. 3 C–D), object exploration was increased (Fig. 4 C–D). This again suggests reduced anxiety, increased exploratory behavior, or both.

$Ca_V2.2$ deficiency significantly delayed disease onset by 18 days compared to SOD1 mice, but did not meaningfully extend survival (Fig. 5). This result suggests that $Ca_V2.2$ influences early pathogenic mechanisms but is insufficient alone to halt disease progression, consistent with the multifactorial nature of ALS (Zarei et al., 2015). Similar visible effects have been reported for edaravone treatment, which improves ALSFRS-R scores without prolonging survival (Jaiswal, 2019).

Histological analysis of the spinal cord, brain, and *M. gastrocnemius* showed that $Cav^{-/-}$ mice did not show changes in NeuN, ChAT, Iba1, GFAP, Bgtx, or SOD1 markers compared with WT mice (Fig. 6 A–O). In contrast, $Cav^{-/-}$-SOD1 mice exhibited typical ALS pathology similar to SOD1 mice, including reduced NeuN and ChAT positive neurons in the ventral horn of the spinal cord and in areas of brain motor nuclei. This reduction is largely because of motor neuron degeneration, a hallmark of the SOD1*G93A mouse model (Gurney et al., 1994). Degeneration was most pronounced in the spinal cord and progressed rostrally (Ravits, 2014). In SOD1 mice, initial pathological symptoms were observed as a reduction in the splay reflex and prominent hindlimb tremor (Mead et al., 2011), with bulbar symptoms evident subsequently (Smittkamp et al., 2008; Fogarty et al., 2024), which is consistent with a spinal-to-bulbar progression in the SOD1*G93A mouse model. Neurodegeneration was accompanied by an inflammatory response. In the spinal cord and brain, $Cav^{-/-}$-SOD1 and SOD1 mice exhibited significantly increased immunoreactive areas of activated glia. Only in the medulla, active microglia were increased in $Cav^{-/-}$-SOD1 mice compared with SOD1 mice. The marker Iba1 is described as an actin-cross-linking protein involved in phagocytosis of activated macrophages and microglia (Ohsawa et al., 2000; Sasaki et al., 2001). In this context, the significantly increased Iba1 signal indicates more active phagocytosis by microglia in the medulla than in the pons or the lumbar spinal cord, potentially depicting the spinal-to-brain propagation discussed. At the end stage, innervation of muscular end plates was lost in SOD1 and $Cav^{-/-}$-SOD1 mice by approximately 50%. This degeneration of ChAT-positive neurons in muscles became evident by the reduced splay from 8 weeks of age in SOD1 mice versus 16 weeks of age in $Cav^{-/-}$-SOD1 mice. In the end, there is no detectable difference between these groups. This conclusion is consistent with Vinsant et al., who showed a reduced motor response in the *M. gastrocnemius* at P47 and the onset of muscle denervation as early as P25 (Vinsant et al., 2013). If the delayed disease onset and diminished splay score sums in $Cav^{-/-}$-SOD1 mice are accompanied by a higher number of innervated muscular endplates should be investigated more closely. In general, at the disease endpoint, the loss of the N-type channels did not reduce inflammatory responses or rescue neurons. As survival was not prolonged in $Cav^{-/-}$-SOD1 mice, histology was not expected to show differences compared with SOD1 mice.

Overexpression of mutated SOD1 causes protein aggregation and ALS-like symptoms in this mouse model (Gurney et al., 1994). SOD1 aggregation was significantly reduced in the brain regions (pons and

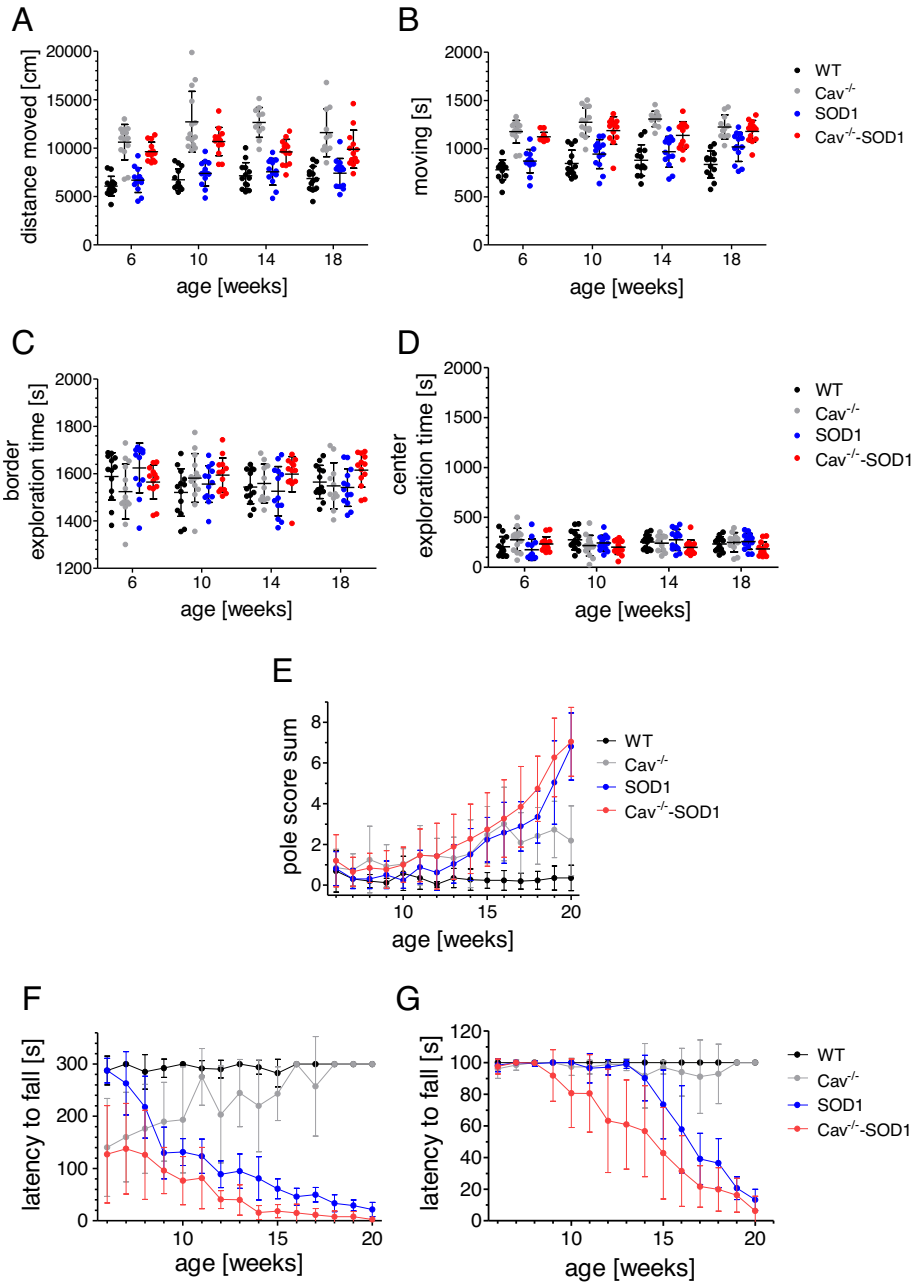

Fig. 3. The additive effect of the $Ca_V2.2$ knockout.
(A–B) $Cav^{-/-}$ and $Cav^{-/-}$-SOD1 mice moved significantly more in the OFT. (C–D) There were no differences in center or border exploration between the genotypes. (E) $Cav^{-/-}$ mice performed worse in the pole test than WT mice. The $Cav^{-/-}$-SOD1 mice developed a progressive deficit mirroring the one of SOD1 mice. (F) In part 1 of the study, $Cav^{-/-}$ mice had initially a lower latency to fall than the WT mice in the hanging wire test. Likewise, $Cav^{-/-}$-SOD1 mice started with a low latency to fall in this test which decreased progressively. (G) After an adjustment of the hanging wire protocol in part 2, $Cav^{-/-}$ mice remained at WT-level. $Cav^{-/-}$-SOD1 mice still performed worse than SOD1 mice. (A–G) Data presented are the mean ± SD. Statistical analysis was performed using two-way RM ANOVA for the effect of genotype and age on the different parameters. (A) $F_{interaction}(9,49) = 1.457$, $p = 0.170$; $F_{genotype}(3,49) = 54.811$, $p < 0.001$; $F_{age}(3,49) = 7.528$, $p < 0.001$; (B) $F_{interaction}(9,49) = 1.275$, $p = 0.256$; $F_{genotype}(3,49) = 49.840$, $p < 0.001$; $F_{age}(3,49) = 7.219$, $p < 0.001$; (C) $F_{interaction}(9,49) = 3.657$, $p < 0.001$; $F_{genotype}(3,49) = 0.860$, $p = 0.468$; $F_{age}(3,49) = 0.494$, $p = 0.687$; (D) $F_{interaction}(9,49) = 3.756$, $p < 0.001$; $F_{genotype}(3,49) = 0.867$, $p = 0.460$; $F_{age}(3,49) = 0.400$, $p = 0.753$. (E) $F_{interaction}(42,49) = 15.373$, $p < 0.001$; $F_{genotype}(3,49) = 22.803$ $p < 0.001$; $F_{age}(14,49) = 75.111$, $p < 0.001$; (F) $F_{interaction}(17, 42) = 15.019$, $p < 0.001$; $F_{genotype}(3,49) = 102.247$, $p < 0.001$; $F_{age}(14,49) = 7.156$, $p < 0.001$; (G) $F_{interaction}(28, 42) = 23.725$, $p < 0.001$; $F_{genotype}(3,49) = 48.980$, $p < 0.001$; $F_{age}(14,49) = 71.934$, $p < 0.001$. (A–E) WT (n = 14, 7♂:7♀), $Cav^{-/-}$ (n = 14, 7♂:7♀), SOD1 (n = 13, 7♂:6♀), $Cav^{-/-}$-SOD1 (n = 14, 8♂:6♀). (F) WT (n = 5, 3♂:2♀), $Cav^{-/-}$ (n = 5, 3♂:2♀), SOD1 (n = 7, 4♂:3♀), $Cav^{-/-}$-SOD1 (n = 5, 3♂:2♀). (G) WT (n = 9, 4♂:5♀), $Cav^{-/-}$ (n = 9, 4♂:5♀), SOD1 (n = 7, 3♂:4♀), $Cav^{-/-}$-SOD1 (n = 9, 4♂:5♀).

medulla) of $Cav^{-/-}$-SOD1 mice but not in the spinal cord (Fig. 6 E, J, O). This observation supports the concept of prion-like propagation (Gosset et al., 2022), although alternative interpretations suggest regional differences in aggregation capacity and toxicity (Gill et al., 2019). Given the presynaptic location of $Ca_V2.2$, its absence may impair vesicle-mediated SOD1 spread (Jurkovicova-Tarabova and Lacinova, 2019), although other propagation pathways likely remain active (Gosset et al., 2022).

Consistent with previous findings in murine neurons (Pieri et al., 2013), we observed a similar increase in $Ca_V2.2$ expression in spinal cord and medulla oblongata tissues from patients with ALS (Fig. 7). Although limited by size from the NBB, this represents the first

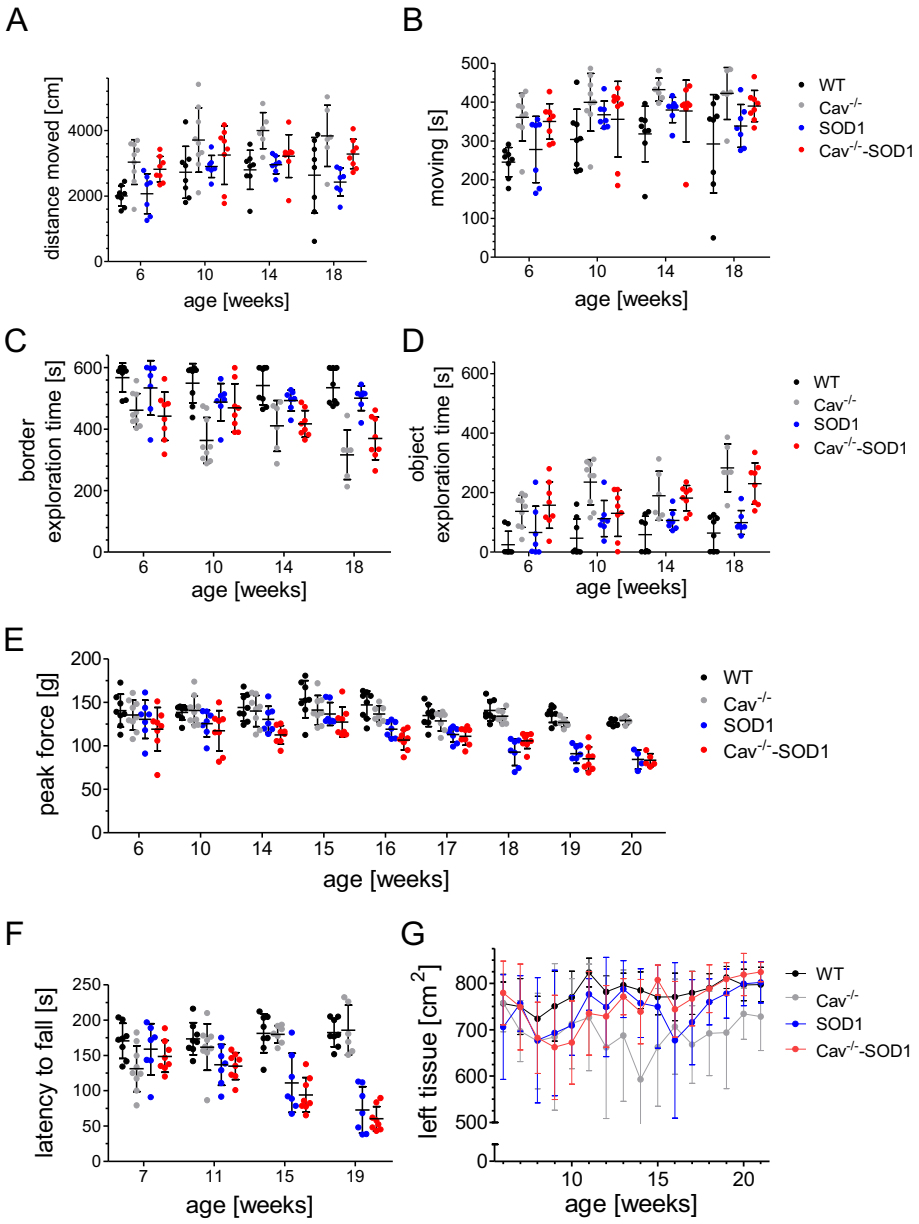

Fig. 4. The non-WT-like behavior of Cav$^{-/-}$ mice.
(A–B) Cav$^{-/-}$ and Cav$^{-/-}$-SOD1 mice moved significantly more in the object exploration test. (C–D) Additionally, they explored the object in the center more than WT mice. (E) Cav$^{-/-}$ mice showed similar peak forces in the grip strength test than WT mice; SOD1 and Cav$^{-/-}$-SOD1 mice progressively lost force in hind limbs. (F) In the rotarod, Cav$^{-/-}$ mice showed similar coordination as WT mice, while SOD1 and Cav$^{-/-}$-SOD1 mice showed decreased latencies to fall. (G) Analysis of the remaining paper tissue area showed that Cav$^{-/-}$ mice gnawed more on paper tissues than any other genotype. (A–G) Data presented are the mean ± SD. Statistical analysis was performed using two-way RM ANOVA for the effect of genotype and on the different parameters. (A) $F_{interaction}(9, 28) = 0.503$, $p = 0.868$; $F_{genotype}(3, 28) = 8.392$, $p < 0.001$; $F_{age}(3, 28) = 10.963$, $p < 0.001$; (B) $F_{interaction}(9, 28) = 0.622$, $p = 0.775$; $F_{genotype}(3, 28) = 7.498$, $p < 0.001$; $F_{age}(3, 28) = 6.664$, $p < 0.001$; (C) $F_{interaction}(9, 28) = 2.090$, $p = 0.040$; $F_{genotype}(3, 28) = 26.063$, $p < 0.001$; $F_{age}(3, 28) = 6.984$, $p < 0.001$; (D) $F_{interaction}(9, 28) = 2.082$, $p = 0.041$; $F_{genotype}(3, 28) = 26.295$, $p < 0.001$; $F_{age}(3, 28) = 7.517$, $p < 0.001$. (E) $F_{interaction}(24, 28) = 2.474$, $p < 0.001$; $F_{genotype}(3, 28) = 56.528$, $p < 0.001$; $F_{age}(8, 28) = 17.593$, $p < 0.001$; (F) $F_{interaction}(9, 28) = 13.502$, $p < 0.001$; $F_{genotype}(3, 28) = 23.549$, $p < 0.001$; $F_{age}(3,49) = 8.440$, $p < 0.001$. (G) $F_{interaction}(28, 45) = 1.523$, $p = 0.020$; $F_{genotype}(3, 28) = 3.219$, $p = 0.038$; $F_{age}(3, 15) = 5.878$, $p < 0.001$. WT (n = 9, 4♂:5♀), Cav$^{-/-}$ (n = 9, 4♂:5♀), SOD1 (n = 7, 3♂:4♀), Cav$^{-/-}$-SOD1 (n = 9, 4♂:5♀).

demonstration of differential $Ca_V2.2$ expression in human ALS brain and spinal cord tissues.

This study has several limitations: First, mechanistic analyses at early disease stages were not performed, despite this being the period of greatest $Ca_V2.2$ effect. In the future, this period has to be the focus when analyzing the influence of $Ca_V2.2$ on ALS pathology. Second, phenotypes in Cav$^{-/-}$ mice, including hyperactivity and seizures, were not fully characterized. Third, the two-part study design may introduce variability, although this was largely not statistically significant. Future studies should focus on early disease stages and refine breeding strategies to account for the non-mendelian inheritance.

Overall, these findings identify $Ca_V2.2$ as a potential modulator of early ALS progression.

5. Conclusion

This study characterized a new Cav$^{-/-}$-SOD1 mouse model and demonstrated that the loss of the $Ca_V2.2$ channel improves early disease phenotypes and delays disease onset. These findings indicate that $Ca_V2.2$ plays a modulatory role in ALS progression, particularly at

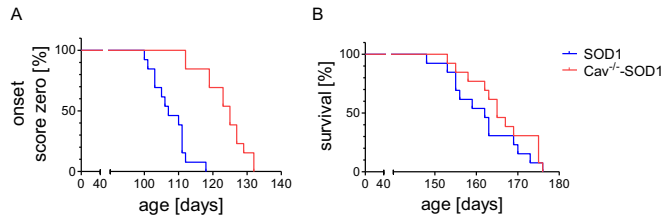

Fig. 5. Comparison of disease onset and survival between SOD1 and $Cav^{-/-}$-SOD mice.
(A) Knockout of the $Ca_V2.2$ channel in the SOD1*G93A mouse model led to a delayed disease onset. (B) In the end, the knockout did not affect survival. (A–B) Statistical analysis was performed using Kaplan-Meier survival analysis and log-rank testing. (A) $p < 0.001$; (B) $p = 0.274$. WT (n = 14, 7♂:7♀), $Cav^{-/-}$ (n = 14, 7♂:7♀), SOD1 (n = 13, 7♂:6♀), $Cav^{-/-}$-SOD1 (n = 14, 8♂:6♀).

disease onset. Increased $Ca_V2.2$ expression in human ALS tissue further supports its clinical relevance and was first demonstrated by post-mortem quantification herein. In addition, the pronounced behavioral phenotype of $Cav^{-/-}$ mice highlights broader roles of this channel in neuronal and behavioral regulation, and calls for a more thorough investigation of the N-type KO mouse model.

CRediT authorship contribution statement

Katharina Wintz: Writing – review & editing, Writing – original draft, Visualization, Methodology, Investigation, Formal analysis, Data curation, Conceptualization. **Paul Luca Lechtape:** Writing – review & editing, Investigation. **Jannes Klenzendorf:** Writing – review & editing, Investigation. **Sarah Schemmert:** Writing – review & editing, Methodology, Conceptualization. **Andrew J. Dingley:** Writing – review & editing. **Antje Willuweit:** Writing – review & editing, Methodology, Conceptualization. **Janine Kutzsche:** Writing – review & editing, Writing – original draft, Supervision, Resources, Project administration,

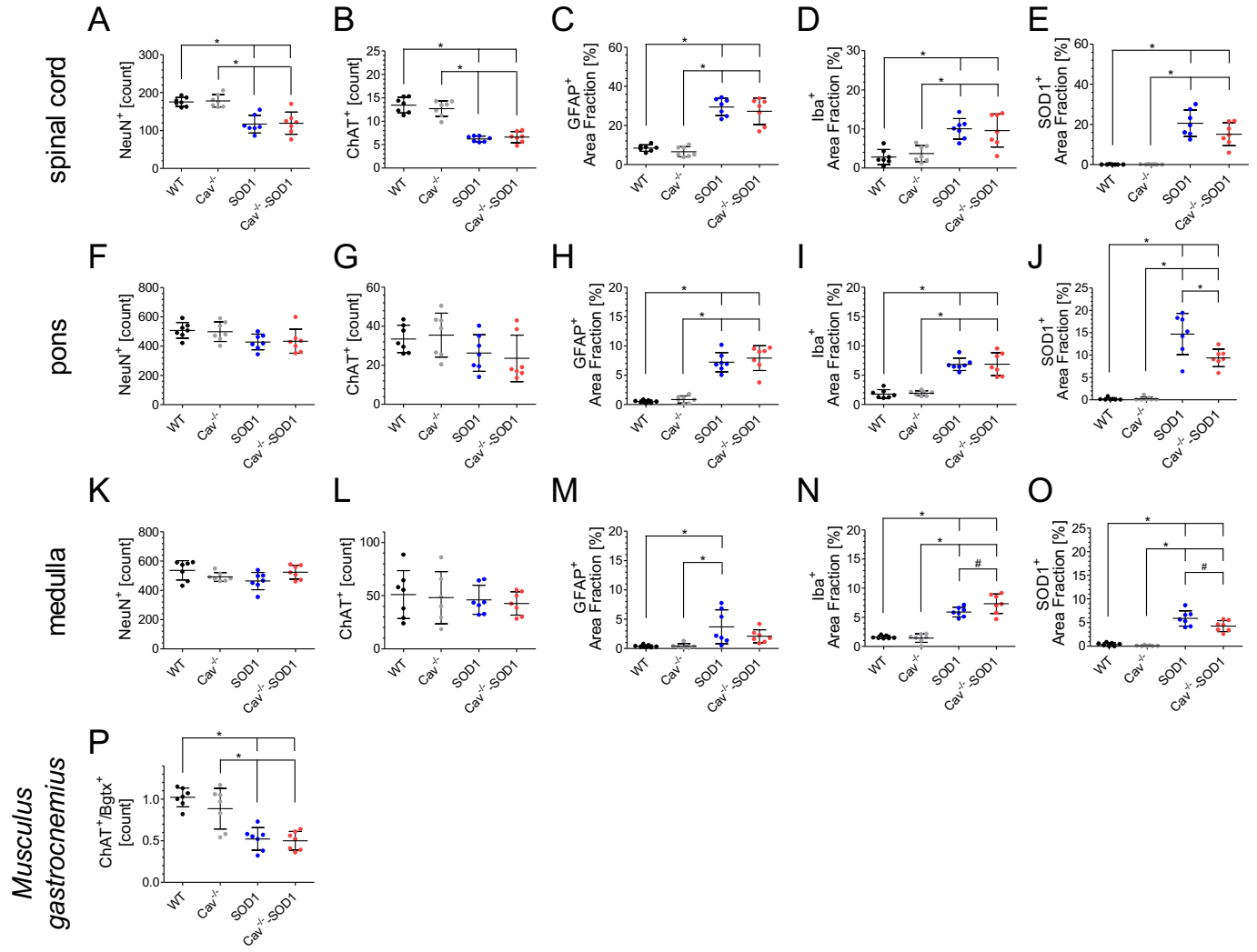

Fig. 6. Histology of the spinal cord and brain (pons, medulla).
(A–D, F–I, K–M) Knockout of the $Ca_V2.2$ channel did not lead to changes in neuronal (NeuN, ChAT) or neuroinflammatory markers (astrocytes, microglia) in the spinal cord, pons, or medulla of $Cav^{-/-}$-SOD1 mice compared with SOD1 mice. (N) Only the Iba^+ area fraction in the medulla was significantly different in $Cav^{-/-}$-SOD1 mice compared with SOD1 mice. (E, J, O) KO of $Ca_V2.2$ reduced SOD1 protein aggregation of $Cav^{-/-}$-SOD1 mice compared with SOD1 mice. (P) The innervation of muscular endplates was investigated with ChAT and Bungarotoxin (Bgtx, nicotinic acetylcholine receptors). KO of $Ca_V2.2$ did not lead to changes in the ChAT/Bgtx-ratio of $Cav^{-/-}$-SOD1 mice compared with SOD1 mice. (A–P) Data are depicted as mean ± SD and were analyzed using one-way ANOVA. (A) $F(3, 24) = 17.745$, $p < 0.001$; (B) $F(3, 24) = 57.185$, $p < 0.001$; (C) $F(3, 24) = 54.914$, $p < 0.001$; (D) $F(3, 24) = 12.353$, $p < 0.001$; (E) $F(3, 24) = 40.677$, $p < 0.001$; (F) $F(3, 24) = 2.911$, $p = 0.055$; (G) $F(3, 24) = 2.232$, $p = 0.110$; (H) $F(3, 24) = 58.595$, $p < 0.001$; (I) $F(3, 24) = 41.741$, $p < 0.001$; (J) $F(3, 24) = 56.842$, $p < 0.001$; (K) $F(3, 24) = 2.801$, $p = 0.062$; (L) $F(3, 24) = 0.246$, $p = 0.861$; (M) $F(3, 24) = 7.096$, $p < 0.001$; (N) $F(3, 24) = 61.579$, $p < 0.001$; (O) $F(3, 24) = 55.980$, $p < 0.001$; (P) $F(3, 24) = 18.495$, $p < 0.001$. If differences between the mean of the groups were detected, post-hoc Holm-Sidak testing was performed. $^*p < 0.001$, $^\#p < 0.05$.

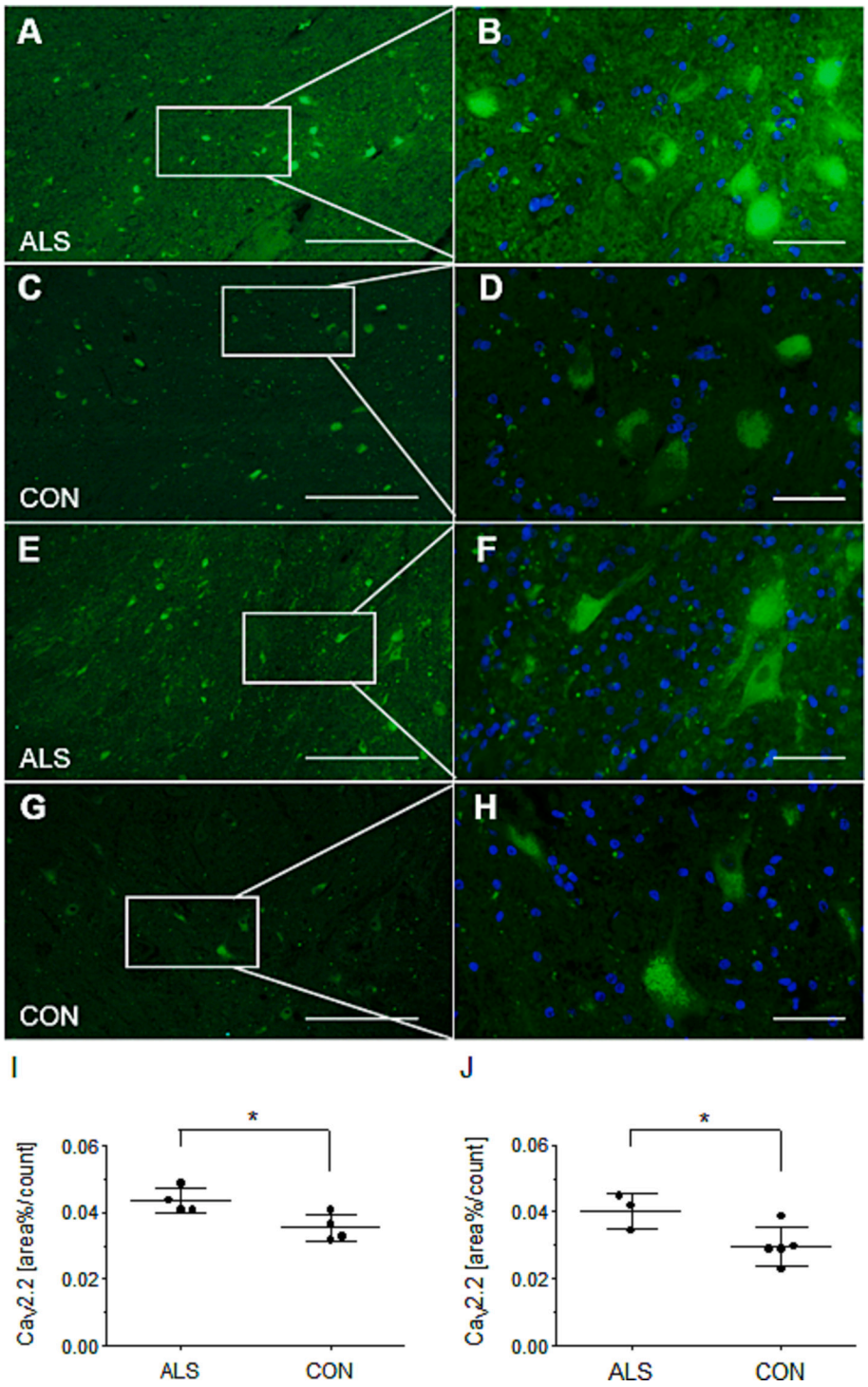

Fig. 7. Quantitative estimation of $Ca_V2.2$ in human samples.
The $Ca_V2.2$ channel (green) was stained in controls (CON) and ALS-diagnosed (ALS) patients in the medulla oblongata (A–D) and spinal cord (E–H). Quantification was conducted using the smaller magnification on the left (scale: 200 μm). Single cells were depicted using the higher magnification on the right (DAPI in blue, scale: 50 μm). $Ca_V2.2$ was quantified in CON and ALS samples of the medulla oblongata (I) and spinal cord (J). The stained area by $Ca_V2.2$ was divided by the cell count per image. (I–J) Data are depicted as mean ± SD. Quantification of $Ca_V2.2$ showed significant difference in both tissues (*t*-test: (I) $p = 0.027$; (J) $p = 0.039$). (For interpretation of the references to colour in this figure legend, the reader is referred to the web version of this article.)

Methodology, Funding acquisition, Formal analysis, Data curation, Conceptualization.

Institutional review board statement

All applicable international, national, and/or institutional guidelines for the care and use of animals were followed. All procedures performed in studies involving animals were in accordance with the ethical standards of the institution. All animal experiments, including details on design, protocols and analysis plan, were performed in accordance with the ARRIVE guidelines, the German Law on the protection of animals (TierSchG §§ 7–9) and with prior approval from the local authority and

ethics committee (Landesamt für Natur, Umwelt und Verbraucherschutz (LANUV), North Rhine-Westphalia, Germany; reference number: AZ 81-02.04.2021.A232 (approval 06/08/2021) and AZ 81-02.04.2021.A243 (approval 30/11/2021)).

Human Samples were ordered from the Netherlands Brain Bank (NBB, open access: www.brainbank.nl, project number 1692). All Material has been collected from donors for or from whom a written informed consent for a brain/spinal cord autopsy and the use of the material and clinical information for research purposes had been obtained by the NBB. The study involving human tissue samples was approved by the ethics committee of the medical faculty of the Heinrich-Heine-University, Düsseldorf (study number: 2022-2154).

Funding

This work was supported by the German Research Foundation (DFG) (project number 519747461).

Declaration of competing interest

The authors declare the following financial interests/personal relationships which may be considered as potential competing interests:

Janine Kutzsche reports financial support was provided by German Research Foundation. Antje Willuweit reports a relationship with Priavoid GmbH that includes: co-founder and employment. Sarah Schemmert reports a relationship with Priavoid GmbH that includes: employment. If there are other authors, they declare that they have no known competing financial interests or personal relationships that could have appeared to influence the work reported in this paper.

Acknowledgments

We thank the animal facility of Forschungszentrum Jülich GmbH for their excellent care.

Appendix A. Supplementary data

Supplementary data to this article can be found online at https://doi.org/10.1016/j.nbd.2026.107396.

Data availability

The data sets used and/or analyzed during the current study are available from the corresponding author on reasonable request.

References

Alexander, G.M., Erwin, K.L., Byers, N., Deitch, J.S., Augelli, B.J., Blankenhorn, E.P., et al., 2004. Effect of transgene copy number on survival in the G93A SOD1 transgenic mouse model of ALS. Mol. Brain Res. 130 (1–2), 7–15. https://doi.org/10.1016/j.molbrainres.2004.07.002.

ALS Association T, 2026. Medications for Treating ALS. https://www.als.org/navigating-als/living-with-als/medications (web archive link, 5 January 2026) accessed. 05.01.2026.

ALSoD A, 2022. Amyotrophic Lateral Sclerosis online Database - ALSoD. https://alsod.ac.uk/ (web archive link, 5 January 2026) (accessed 05.01.2026).

Beuckmann, C.T., Sinton, C.M., Miyamoto, N., Ino, M., Yanagisawa, M., 2003. N-type calcium channel α1B subunit (CaV2.2) Knock-out mice display hyperactivity and vigilance state differences. J. Neurosci. 23 (17), 6793–6797. https://doi.org/10.1523/jneurosci.23-17-06793.2003.

Chang, Q., Martin, L.J., 2016. Voltage-gated calcium channels are abnormal in cultured spinal motoneurons in the G93A-SOD1 transgenic mouse model of ALS. Neurobiol. Dis. 93, 78–95. https://doi.org/10.1016/j.nbd.2016.04.009.

Dunkelmann, T., Schemmert, S., Honold, D., Teichmann, K., Butzküven, E., Demuth, H.-U., et al., 2018. Comprehensive characterization of the pyroglutamate amyloid-β induced motor neurodegenerative phenotype of TBA2.1 mice. J. Alzheimer's Dis 63 (1), 115–130. https://doi.org/10.3233/JAD-170775.

Fogarty, M.J., Drieberg-Thompson, J.R., Bellingham, M.C., Noakes, P.G., 2024. Timeline of hypoglossal motor neuron death and intrinsic tongue muscle denervation in high-copy number SOD1^{G93A} mice. Front. Neurol. 15, 1422943. https://doi.org/10.3389/fneur.2024.1422943.

Gill, C., Phelan, J.P., Hatzipetros, T., Kidd, J.D., Tassinari, V.R., Levine, B., et al., 2019. SOD1-positive aggregate accumulation in the CNS predicts slower disease progression and increased longevity in a mutant SOD1 mouse model of ALS. Sci. Rep. 9 (1), 6724. https://doi.org/10.1038/s41598-019-43164-z.

Gorman, K.M., Meyer, E., Grozeva, D., Spinelli, E., McTague, A., Sanchis-Juan, A., et al., 2019. Bi-allelic loss-of-function CACNA1B mutations in progressive epilepsy-dyskinesia. Am. J. Hum. Genet. 104 (5), 948–956. https://doi.org/10.1016/j.ajhg.2019.03.005.

Gosset, P., Camu, W., Raoul, C., Mezghrani, A., 2022. Prionoids in amyotrophic lateral sclerosis. Brain Commun. 4 (3). https://doi.org/10.1093/braincomms/fcac145.

Gurney, M.E., Pu, H., Chiu, A.Y., Dal Canto, M.C., Polchow, C.Y., Alexander, D.D., et al., 1994. Motor neuron degeneration in mice that express a human cu, Zn superoxide dismutase mutation. Science 264 (5166), 1772–1775. https://doi.org/10.1126/science.8209258.

Hardiman, O., Van Den Berg, L.H., Kiernan, M.C., 2011. Clinical diagnosis and management of amyotrophic lateral sclerosis. Nat. Rev. Neurol. 7 (11), 639–649. https://doi.org/10.1038/nrneurol.2011.153.

Hatakeyama, S., Wakamori, M., Ino, M., Miyamoto, N., Takahashi, E., Yoshinaga, T., et al., 2001. Differential nociceptive responses in mice lacking the α1B subunit of n-type ca2+ channels. Neuroreport 12 (11), 2423–2427. https://doi.org/10.1097/00001756-200108080-00027.

Huntula, S., Saegusa, H., Wang, X., Zong, S., Tanabe, T., 2019. Involvement of n-type ca2 + channel in microglial activation and its implications to aging-induced exaggerated cytokine response. Cell Calcium 82, 102059. https://doi.org/10.1016/j.ceca.2019.102059.

Ino, M., Yoshinaga, T., Wakamori, M., Miyamoto, N., Takahashi, E., Sonoda, J., et al., 2001. Functional disorders of the sympathetic nervous system in mice lacking the α1B subunit (CaV2.2) of n-type calcium channels. Proc. Natl. Acad. Sci. 98 (9), 5323–5328. https://doi.org/10.1073/pnas.081089398.

Iwasaki, S., Momiyama, A., Uchitel, O.D., Takahashi, T., 2000. Developmental changes in calcium channel types mediating central synaptic transmission. J. Neurosci. 20 (1), 59–65. https://doi.org/10.1523/JNEUROSCI.20-01-00059.2000.

Jaiswal, M.K., 2019. Riluzole and edaravone: a tale of two amyotrophic lateral sclerosis drugs. Med. Res. Rev. 39 (2), 733–748. https://doi.org/10.1002/med.21528.

Jiang, K., Yang, L.-T., Xue, M., 2025. Breaking the synaptic vesicle cycle: mechanistic insights into presynaptic dysfunctions in epilepsy. Epilepsy Curr. 25 (2), 119–124. https://doi.org/10.1177/15357597251317898.

Jurkovicova-Tarabova, B., Lacinova, L., 2019. Structure, function and regulation of CaV2.2 n-type calcium channels. Gen. Physiol. Biophys. 38 (2), 101–110. https://doi.org/10.4149/gpb_2019004.

Ketabforoush, A., Faghihi, F., Azedi, F., Ariaei, A., Habibi, M.A., Khalili, M., et al., 2024. Sodium phenylbutyrate and tauroursodeoxycholic acid: a story of hope turned to disappointment in amyotrophic lateral sclerosis treatment. Clin. Drug Investig. 44 (7), 495–512. https://doi.org/10.1007/s40261-024-01371-1.

Kutzsche, J., Guzman, G.A., Willuweit, A., Kletke, O., Wollert, E., Gering, I., et al., 2024. An orally available Ca_V2. 2 calcium channel inhibitor for the treatment of neuropathic pain. Br. J. Pharmacol. 181 (12), 1734–1756. https://doi.org/10.1111/bph.16309.

Masrori, P., Van Damme, P., 2020. Amyotrophic lateral sclerosis: a clinical review. Eur. J. Neurol. 27 (10), 1918–1929. https://doi.org/10.1111/ene.14393.

Matsuura, K., Kabuto, H., Makino, H., Ogawa, N., 1997. Pole test is a useful method for evaluating the mouse movement disorder caused by striatal dopamine depletion. J. Neurosci. Methods 73 (1), 45–48. https://doi.org/10.1016/S0165-0270(96)02211-X.

Mead, R.J., Bennett, E.J., Kennerley, A.J., Sharp, P., Sunyach, C., Kasher, P., et al., 2011. Optimised and rapid pre-clinical screening in the SOD1^{G93A} transgenic mouse model of amyotrophic lateral sclerosis (ALS). PLoS One 6 (8), e23244. https://doi.org/10.1371/journal.pone.0023244.

Miller, T.M., Cudkowicz, M.E., Genge, A., Shaw, P.J., Sobue, G., Bucelli, R.C., et al., 2022. Trial of antisense oligonucleotide tofersen for SOD1 ALS. N. Engl. J. Med. 387 (12), 1099–1110. https://doi.org/10.1056/NEJMoa2204705.

Mori, Y., Nishida, M., Shimizu, S., Ishii, M., Yoshinaga, T., Ino, M., et al., 2002. Ca2+ channel α1B subunit (CaV2.2) knockout mouse reveals a predominant role of N-type channels in the sympathetic regulation of the circulatory system. Trends Cardiovasc. Med. 12 (6), 270–275. https://doi.org/10.1016/S1050-1738(02)00173-1.

Nakagawasai, O., Onogi, H., Mitazaki, S., Sato, A., Watanabe, K., Saito, H., et al., 2010. Behavioral and neurochemical characterization of mice deficient in the n-type Ca2+ channel α1B subunit. Behav. Brain Res. 208 (1), 224–230. https://doi.org/10.1016/j.bbr.2009.11.042.

Ohsawa, K., Imai, Y., Kanazawa, H., Sasaki, Y., Kohsaka, S., 2000. Involvement of iba1 in membrane ruffling and phagocytosis of macrophages/microglia. J. Cell Sci. 113 (17), 3073–3084. https://doi.org/10.1242/jcs.113.17.3073.

Paganoni, S., Macklin, E.A., Hendrix, S., Berry, J.D., Elliott, M.A., Maiser, S., et al., 2020. Trial of sodium phenylbutyrate–taurursodiol for amyotrophic lateral sclerosis. N. Engl. J. Med. 383 (10), 919–930. https://doi.org/10.1056/NEJMoa1916945.

Paganoni, S., Hendrix, S., Dickson, S.P., Knowlton, N., Macklin, E.A., Berry, J.D., et al., 2021. Long-term survival of participants in the CENTAUR trial of sodium phenylbutyrate-taurursodiol in amyotrophic lateral sclerosis. Muscle Nerve 63 (1), 31–39. https://doi.org/10.1002/mus.27091.

Park, H.R., Yang, E.J., 2021. Oxidative stress as a therapeutic target in amyotrophic lateral sclerosis: opportunities and limitations. Diagnostics 11 (9), 1546. https://doi.org/10.3390/diagnostics11091546.

Pieri, M., Caioli, S., Canu, N., Mercuri, N.B., Guatteo, E., Zona, C., 2013. Over-expression of n-type calcium channels in cortical neurons from a mouse model of amyotrophic lateral sclerosis. Exp. Neurol. 247, 349–358. https://doi.org/10.1016/j.expneurol.2012.11.002.

Post, J., Kogel, V., Schaffrath, A., Lohmann, P., Shah, N.J., Langen, K.-J., et al., 2021a. A novel anti-inflammatory d-peptide inhibits disease phenotype progression in an ALS mouse model. Molecules 26 (6), 1590. https://doi.org/10.3390/molecules26061590.

Post, J., Schaffrath, A., Gering, I., Hartwig, S., Lehr, S., Shah, N.J., et al., 2021b. Oral treatment with RD2RD2 impedes development of motoric phenotype and delays symptom onset in SOD1G93A transgenic mice. Int. J. Mol. Sci. 22 (13), 7066. https://doi.org/10.3390/ijms22137066.

Ravits, J., 2014. Focality, stochasticity and neuroanatomic propagation in ALS pathogenesis. Exp. Neurol. 262, 121–126. https://doi.org/10.1016/j.expneurol.2014.07.021.

Saegusa, H., Kurihara, T., Zong, S., Kazuno, A.-a., Matsuda, Y., Nonaka, T., et al., 2001. Suppression of inflammatory and neuropathic pain symptoms in mice lacking the n-type Ca2+ channel. EMBO J. 20 (10), 2349–2356. https://doi.org/10.1093/emboj/20.10.2349.

Sasaki, Y., Ohsawa, K., Kanazawa, H., Kohsaka, S., Imai, Y., 2001. Iba1 is an actin-cross-linking protein in macrophages/microglia. Biochem. Biophys. Res. Commun. 286 (2), 292–297. https://doi.org/10.1006/bbrc.2001.5388.

Schneider, C.A., Rasband, W.S., Eliceiri, K.W., 2012. NIH image to ImageJ: 25 years of image analysis. Nat. Methods 9 (7), 671–675. https://doi.org/10.1038/nmeth.2089.

Smittkamp, S.E., Brown, J.W., Stanford, J.A., 2008. Time-course and characterization of orolingual motor deficits in B6SJL-Tg (SOD1-G93A) 1Gur/J mice. Neuroscience 151 (2), 613–621. https://doi.org/10.1016/j.neuroscience.2007.10.017.

Suzuki, Y.-I., Shibuya, K., Misawa, S., Suichi, T., Tsuneyama, A., Kojima, Y., et al., 2022. Relationship between motor cortical and peripheral axonal hyperexcitability in amyotrophic lateral sclerosis. J. Neurol. Neurosurg. Psychiatry 93 (10), 1074–1079. https://doi.org/10.1136/jnnp-2021-328550.

Ting, J.T., Feng, G., 2008. Glutamatergic synaptic dysfunction and obsessive-compulsive disorder. Curr. Chem. Genomics 2, 62. https://doi.org/10.2174/1156652323167082408280635 27.

Vinsant, S., Mansfield, C., Jimenez-Moreno, R., Moore, V.D.G., Yoshikawa, M., Hampton, T.G., et al., 2013. Characterization of early pathogenesis in the SOD1G93A mouse model of ALS: Part I, background and methods. Brain Behav. 3 (4), 335–350. https://doi.org/10.1002/brb3.143.

Wintz, K., Post, J., Langen, K.-J., Willbold, D., Willuweit, A., Kutzsche, J., 2023. Oral treatment with d-RD2RD2 impedes early disease mechanisms in SOD1*G93A transgenic mice but does not prolong survival. Biomedicines 11 (4), 995. https://doi.org/10.3390/biomedicines11040995.

Würbel, H., Chapman, R., Rutland, C., 1998. Effect of feed and environmental enrichment on development of stereotypic wire-gnawing in laboratory mice. Appl. Anim. Behav. Sci. 60 (1), 69–81. https://doi.org/10.1016/S0168-1591(98)00150-6.

Xiao, Y., Huang, C., Wang, J., Lin, Y., Quan, D., Zheng, H., 2025. Neurobiological differences in early-onset obsessive-compulsive disorder: a study of the glutamatergic system based on functional magnetic resonance spectroscopy. J. Affect. Disord. 379, 755–763. https://doi.org/10.1016/j.jad.2025.03.088.

You, J., Youssef, M.M., Santos, J.R., Lee, J., Park, J., 2023. Microglia and astrocytes in amyotrophic lateral sclerosis: disease-associated states, pathological roles, and therapeutic potential. Biology 12 (10), 1307. https://doi.org/10.3390/biology12101307.

Zarei, S., Carr, K., Reiley, L., Diaz, K., Guerra, O., Altamirano, P.F., et al., 2015. A comprehensive review of amyotrophic lateral sclerosis. Surg. Neurol. Int. 6. https://doi.org/10.4103/2152-7806.169561.